Eur. Phys. J. C (2017) 77:751
https://doi.org/10.1140/epjc/s10052-017-5140-y

THE EUROPEAN PHYSICAL JOURNAL C

Regular Article - Experimental Physics

Measurements of the associated production of a Z boson and b jets in pp collisions at $\sqrt{s} = 8$ TeV

CMS Collaboration*

CERN, 1211 Geneva 23, Switzerland

Received: 20 November 2016 / Accepted: 14 August 2017 / Published online: 8 November 2017

Abstract Measurements of the associated production of a Z boson with at least one jet originating from a b quark in proton–proton collisions at $\sqrt{s} = 8$ TeV are presented. Differential cross sections are measured with data collected by the CMS experiment corresponding to an integrated luminosity of 19.8 fb^{-1}. Z bosons are reconstructed through their decays to electrons and muons. Cross sections are measured as a function of observables characterizing the kinematics of the b jet and the Z boson. Ratios of differential cross sections for the associated production with at least one b jet to the associated production with any jet are also presented. The production of a Z boson with at least two b jets is investigated, and differential cross sections are measured for the dijet system. Results are compared to theoretical predictions, testing two different flavour schemes for the choice of initial-state partons.

1 Introduction

The associated production of vector bosons and jets (V+jets) in hadronic collisions is a large background source in measurements of several standard model (SM) processes, Higgs boson studies, and many searches for physics beyond the SM. Its description constitutes an important benchmark for perturbative quantum chromodynamics (pQCD) predictions. Differential cross sections as a function of kinematic observables characterizing V+jets topologies are sensitive to the contributions from both the hard scattering process and the associated soft QCD radiation, as well as to the parton distribution functions (PDFs). Among the V+jets processes, the case in which a Z/γ^* boson is produced in association with b quarks, $pp \to Z + (\geq 1b)$, hereafter denoted as Z(1b), is particularly interesting. Antiquarks are also assumed in the notation, and the Z/γ^* interference contribution is considered to be part of the process. Within the SM, the Z(1b) final state is the dominant background for studies of the associated production of Higgs and Z bosons, in which the Higgs boson decays into a $b\bar{b}$ pair [1]. Many physics scenarios beyond the SM predict final states with b quarks and Z bosons: new generations of heavy quarks (b', t') decaying into Z(1b) [2], supersymmetric Higgs bosons produced in association with b quarks [3], and extended SM scenarios with additional SU(2) doublets with enhanced $Zb\bar{b}$ coupling [4]. The study of the associated production of Z bosons and b quark jets may also provide information useful in describing an analogous process where a W boson is produced, which is more difficult to measure because of higher background contamination.

This paper presents measurements of associated production of a Z boson and b quark jets using proton–proton collision data at 8 TeV collected with the CMS detector, corresponding to an integrated luminosity of 19.8 fb^{-1}. The Z boson is reconstructed through its leptonic decay into an electron or muon pair, while the presence of b quarks is inferred from the characteristics of jets (denoted as b jets) that originate from their hadronization products and subsequent decays. In order to characterize Z(1b) production, fiducial differential cross sections are measured as a function of five kinematic observables: the transverse momentum p_T and pseudorapidity η of the highest-p_T b jet, the Z boson p_T, the scalar sum of the transverse momenta of all jets regardless of the flavour of the parton producing them (H_T), and the azimuthal angular difference between the direction of the Z boson and the highest-p_T b jet ($\Delta\phi_{Zb}$). Ratios of the differential cross sections for Z(1b) and Z+jets production, inclusive in jet flavour, are also measured as a function of these five observables. The cancellation of several systematic uncertainties in the cross section ratio allows an even more precise comparison with theory than the differential cross sections themselves.

Events with at least two b jets, henceforth Z(2b), contribute as background sources to other SM and beyond-SM processes. The production dynamics of this kind of event are studied through the measurement of the fiducial differential cross section as a function of observables characterizing the kinematic properties of the dijet system formed by the lead-

* e-mail: cms-publication-committee-chair@cern.ch

ing and subleading (in p_T) b jets: the p_T of these two jets; the Z boson p_T; the invariant masses of the bb and Zbb systems (M_{bb} and M_{Zbb} respectively); the angle $\Delta\phi_{bb}$ between the two b jets in the plane transverse to the beam axis and their separation in the η–ϕ plane (ΔR_{bb}); the distance in the η–ϕ plane between the Z boson and the closer b jet (ΔR_{Zb}^{min}); and the asymmetry in the distances in the η–ϕ plane between the Z boson and the closer versus farther b jets (A_{Zbb}).

Previously, the cross section for the associated production of Z bosons and b jets was measured in proton–antiproton collisions by the CDF [5] and D0 [6] Collaborations at the Fermilab Tevatron and in proton–proton collisions at a centre-of-mass energy of 7 TeV by the ATLAS [7] and CMS [8] Collaborations at the CERN LHC. The CMS Collaboration also studied Z(2b) production by explicitly reconstructing b hadron decays [9], in order to explore the region where b quarks are emitted in an almost collinear topology. Previous measurements of the ratio of the Z(1b) to the Z+jets inclusive cross section were published by the D0 Collaboration [10].

The paper is organized as follows: Sect. 2 is dedicated to the description of the CMS apparatus and Sect. 3 to the data and simulated samples used in the analysis. Section 4 discusses the lepton, jet, and b jet reconstruction and the event selection. Section 5 discusses background estimation, while Sect. 6 is dedicated to the description of the unfolding procedure to correct data for detector effects. Section 7 presents a discussion of the systematic uncertainties. In Sect. 8 the measured differential cross sections and the corresponding ratios are presented, together with a discussion of the comparison with theoretical predictions. Finally, the results are summarized in Sect. 9.

2 The CMS detector

A detailed description of the CMS detector, together with the definition of the coordinate system used and the relevant kinematic variables, can be found in Ref. [11]. The central feature of the CMS apparatus is a superconducting solenoid of 6 m internal diameter. The field volume houses a silicon tracker, a crystal electromagnetic calorimeter (ECAL), and a brass and scintillator hadron calorimeter (HCAL), each composed of a barrel and two endcap sections. The magnet flux-return yoke is instrumented with muon detectors. The silicon tracker measures charged particles within the pseudorapidity range $|\eta| < 2.5$. It consists of 1440 silicon pixel and 15 148 silicon strip detector modules and is located in the 3.8 T field of the superconducting solenoid. For non-isolated particles of $1 < p_T < 10$ GeV and $|\eta| < 1.4$, the track resolutions are typically 1.5% in p_T and 25–90 (45–150) μm in the transverse (longitudinal) impact parameter [12]. The electron momentum is estimated by combining the energy measurement in the ECAL with the momentum measurement in the tracker. The momentum resolution for electrons with $p_T \approx 45$ GeV from $Z \to ee$ decays ranges from 1.7% for nonshowering electrons in the barrel region to 4.5% for showering electrons in the endcaps [13]. Muons are measured in the pseudorapidity range $|\eta| < 2.4$, with detection planes made using three technologies: drift tubes, cathode strip chambers, and resistive plate chambers. Matching muons to tracks measured in the silicon tracker results in a relative transverse momentum resolution for muons with $20 < p_T < 100$ GeV of 1.3–2.0% in the barrel and better than 6% in the endcaps. The p_T resolution in the barrel is better than 10% for muons with p_T up to 1 TeV [14]. Forward calorimeters extend the pseudorapidity coverage provided by the barrel and endcap detectors.

The CMS detector uses a two-level trigger system. The first level of the system, composed of custom hardware processors, uses information from the calorimeters and muon detectors to select the most interesting events in a fixed time interval of less than 4 μs. The high-level trigger processor farm further decreases the event rate from around 100 kHz to less than 1 kHz before data storage.

3 Event simulation

The associated production of a Z boson and jets is experimentally reconstructed as two opposite-sign same-flavour electrons or muons accompanied by jets and can be mimicked by various background sources: $t\bar{t}$ events, dibosons (WW, WZ, ZZ) and W bosons produced in association with jets, single top quark events, as well as Z+jets events in which the Z boson decays into $\tau^+\tau^-$. Diboson events with a leptonic Z boson decay and jets produced in the hadronic decay of the other vector boson are not considered as part of the signal. Samples of simulated events are used to model both the signal and the background processes. The MadGraph 5.1.3.30 [15] event generator is used to simulate Z+jets (including jets from b quarks), W+jets, and $t\bar{t}$ events; this generator implements a leading-order (LO) matrix element calculation with up to four (three) additional partons in the final state for V+jets ($t\bar{t}$) events, using the CTEQ6L1 PDF set [16], which is based on the five flavour scheme (5FS). A detailed discussion is given in Sect. 8.2. The parton-level events are interfaced with pythia version 6.424 [17] for parton showering, hadronization, and description of the multiple-parton interactions (MPIs). The pythia6 Z2* tune, which is based on the CTEQ6L1 PDF set, is used [18]. The matrix element and parton shower calculations are matched using the k_t-MLM algorithm [19]. The cross section inclusive in jet multiplicity is rescaled to its next-to-next-to-leading-order (NNLO) prediction, computed with fewz 3.1 [20,21] for the Z+jets and W+jets processes, and with the calculation of Ref. [22] for the $t\bar{t}$ process. To study systematic uncertainties, signal

events are also generated using MADGRAPH5_aMC@NLO [23] version 2.2.1, with next-to-leading-order (NLO) matrix elements for zero, one, and two additional partons merged with the FXFX algorithm [24], interfaced with PYTHIA version 8.205 [25] for showering and hadronization. In this case the NNPDF 3.0 NLO PDF set [26] is used. Depending on the flavours included in the matrix element calculation of the event or produced in the parton shower through gluon splitting, the inclusive Z+jets sample can be divided into Z+b quark, c quark, and light-flavour (u, d, s quark and gluon) jet subsamples. As explained in Sect. 6, the jet flavour identification is based on the particle content of the final state.

Diboson events are simulated with PYTHIA6, and the inclusive cross section rescaled to the NLO prediction provided by MCFM [27]. The single top quark contribution is evaluated using POWHEG-BOX version 1.0 [28–32] interfaced with PYTHIA6 for parton showering, hadronization, and MPI description. The contribution of multijet events is evaluated using PYTHIA6 generated events and found to be negligible.

Generated events are processed with a simulation of the CMS detector based on the GEANT4 toolkit [33]. Signals induced by additional pp interactions in the same or adjacent bunch crossings, referred to as pileup, are simulated using events generated with PYTHIA6. The pileup distribution in simulation is adjusted in order to reproduce the collision rates observed in data. During the 2012 data taking, the average pileup rate was about 21 interactions per bunch crossing.

4 Event selection

The analysis is based on an online trigger selection requiring events to contain a pair of electron or muon candidates with asymmetric minimum thresholds on their transverse momenta. These threshold settings depended on the instantaneous luminosity and reached maximum values of 17 GeV for the leading lepton and 8 GeV for the subleading one. Events are required to contain a Z boson, reconstructed through its decay into an electron or muon pair, produced in association with at least one or at least two hadronic jets. For the Z(1b) and Z(2b) event selections the jets are also required to be identified as originating from the hadronization of a b quark.

All the measured particles are reconstructed using the particle-flow (PF) algorithm [34,35]. The particle-flow event algorithm reconstructs and identifies each individual particle with an optimized combination of information from the various elements of the CMS detector. The energy of photons is obtained directly from the ECAL measurement, corrected for zero-suppression effects. The energy of electrons is evaluated from a combination of the electron momentum at the primary interaction vertex as determined by the tracker, the energy of the corresponding ECAL cluster, and the energy sum of all bremsstrahlung photons spatially compatible with originating from the electron track. The transverse momentum of the muons is obtained from the curvature of the corresponding track. The energy of charged hadrons is determined from a combination of the momentum measured in the tracker and the matching ECAL and HCAL energy deposits, corrected for zero-suppression effects and for the response functions of the calorimeters to hadronic showers. Finally, the energy of neutral hadrons is obtained from the corresponding corrected ECAL and HCAL energies.

The reconstructed leptons selected as candidate decay products of the Z boson must match those that triggered the event and must be associated with the primary vertex of the event, defined as the reconstructed vertex with the largest sum of p_{T}^2 of its constituent tracks. Reconstructed electrons must satisfy a set of selection criteria designed to minimize misidentification at a desired efficiency level [13]; the discriminating observables include the measured shower shape in the ECAL and the spatial matching between the electromagnetic deposit in the calorimeter and the reconstructed track associated with it. Additional requirements on electron tracks are used to reject products of photon conversions. Electron isolation criteria exploit the full PF-based event reconstruction, using particles within a cone around the electron direction with radius $\Delta R = \sqrt{(\Delta\phi)^2 + (\Delta\eta)^2} = 0.3$. The isolation requirement is defined by $I_{\mathrm{rel}} = (I_{\mathrm{charged}} + I_{\mathrm{photon}} + I_{\mathrm{neutral}})/p_{\mathrm{T}}^{\mathrm{e}} < 0.15$, where I_{charged} is the scalar p_{T} sum of all the charged hadrons, I_{photon} is the scalar p_{T} sum of all the photons, and I_{neutral} the scalar sum of p_{T} of all the neutral hadrons in the cone of interest. The notation $p_{\mathrm{T}}^{\mathrm{e}}$ refers to the transverse momentum of the reconstructed electron. Pileup can add extra particles, which affect the isolation variable. Accordingly, only charged particles originating from the reconstructed primary vertex are used in the calculation of I_{charged}. The photon and neutral hadronic contribution to the isolation variable coming from pileup is subtracted using the jet area approach [36]. Electrons must have $p_{\mathrm{T}}^{\mathrm{e}} > 20$ GeV and be reconstructed within the pseudorapidity range $|\eta| < 1.44$ and $1.57 < |\eta| < 2.4$, which exclude the barrel-endcap transition region.

Muon identification criteria are based on the fit quality for tracks measured in the tracker and the muon detector [14]. Further selection criteria are added in order to reject muons from cosmic rays. Muon isolation is computed using all particles reconstructed by the PF algorithm within a cone of radius $\Delta R = 0.4$ around the muon direction, requiring $I_{\mathrm{rel}} = (I_{\mathrm{charged}} + I_{\mathrm{photon}} + I_{\mathrm{neutral}})/p_{\mathrm{T}}^{\mu} < 0.2$. Muons must have $p_{\mathrm{T}}^{\mu} > 20$ GeV and $|\eta| < 2.4$. As in the case of electrons, charged particles not originating from the primary vertex are excluded from the isolation calculation. The pileup contribution to I_{photon} and I_{neutral} is estimated as half of the corresponding charged hadronic component and is subtracted in the definition of the I_{rel} variable.

The efficiencies for lepton trigger, reconstruction, identification, and isolation are measured with the "tag-and-probe" technique [37] as a function of the lepton η and p_{T}. A sample of events containing a Z boson decaying into $\mathrm{e^+e^-}$ or $\mu^+\mu^-$ is used for these studies. Efficiency corrections ("scale factors") of up to 1.2% (7.3%), dependent on lepton p_{T} and η, are applied to account for differences in the estimated efficiencies between data and simulation in the electron (muon) channel.

The pair of selected same-flavour, opposite-sign, highest-p_{T} isolated leptons is retained as a Z boson candidate if the invariant mass $M_{\ell\ell}$ of the pair lies within the 71–111 GeV mass interval. The overall efficiency of the trigger and event selection within the fiducial acceptance is 88% for dimuons and 58% for dielectrons.

Jets are reconstructed using the anti-k_{t} algorithm [38,39] with a distance parameter of 0.5. In order to suppress the contribution from pileup interactions, charged particles not associated with the primary vertex are excluded from the clustering. Jets are required to be in the tracking acceptance region $|\eta| < 2.4$ and to have $p_{\mathrm{T}} > 30$ GeV, thereby reducing the contribution from the underlying event to less than 5%, where jets have a softer p_{T} spectrum compared to jets from the hard scattering process. Jets with a distance $\Delta R < 0.5$ from the closer lepton used for the Z boson decay reconstruction are not considered in the analysis. The jet energy scale (JES) is calibrated using a factorized approach as described in Refs. [40,41]. The jet energy resolution (JER) in data is known to be worse than in the simulation; therefore the simulated resolution is degraded to compensate for this effect as a function of the jet kinematics [40,41].

Jets from b quarks are identified using the combined secondary vertex (CSV) b tagging algorithm [42], a multivariate classifier that makes use of information about reconstructed secondary vertices as well as the impact parameters of the associated tracks with respect to the primary vertex to discriminate b jets from c and light-flavour jets. The threshold applied to the discriminating variable gives a b tagging efficiency of about 50% and a misidentification probability of 0.1% for light jets and 1% for c jets. Scale factors, measured in multijet events and dependent on jet p_{T}, are used to correct the b, c, and light-flavour jet efficiencies in the simulation to match those observed in the data [42]. The scale factors for b jets are determined using samples of events enriched in such a flavour of jets. This enrichment is obtained including both multijet events containing a muon geometrically associated with a jet, with high probability of originating from the semileptonic decay of a b hadron, and leptonic and semileptonic $\mathrm{t\bar{t}}$ events, where the leading p_{T} jets are usually b jets. The scale factors are around 0.93, slowly decreasing for jets with p_{T} above 120 GeV. The scale factors for c jets are assumed the same as for b jets, with an uncertainty twice as large. Relatively pure samples of c jets from $\mathrm{W}+\mathrm{c}$ events, selected using identified muons within the jet, are used to validate this assumption. For light-flavour jets, the same CSV algorithm yields scale factors between 1.1 and 1.4, depending on the jet p_{T}. The calculation is based on tracks with negative signed impact parameter and secondary vertices with negative signed decay lengths, where the sign is defined by the relative direction of the jet and the particle momentum. Finally, events are selected if they contain a Z boson candidate and at least one b-tagged jet.

The missing transverse momentum vector $\vec{p}_{\mathrm{T}}^{\,\mathrm{miss}}$ is defined as the projection on the plane perpendicular to the beams of the negative vector sum of the momenta of all reconstructed particles in an event. Its magnitude is referred to as $E_{\mathrm{T}}^{\mathrm{miss}}$. The $E_{\mathrm{T}}^{\mathrm{miss}}$ significance, introduced in Refs. [43,44], offers an event-by-event assessment of the consistency of the observed missing energy with zero, given the reconstructed content of the event and known measurement resolutions. In order to suppress the background contamination from $\mathrm{t\bar{t}}$ production, events with $E_{\mathrm{T}}^{\mathrm{miss}}$ significance greater than 30 are vetoed. This requirement provides a 13% $\mathrm{t\bar{t}}$ background rejection with no loss in signal efficiency.

The Z(1b) event selection described above yields 26443 (36843) events for the dielectron (dimuon) channels. The exclusive b-tagged jet multiplicity and invariant mass distributions of the same flavour dilepton are presented in Figs. 1 and 2, for the Z(1b) event selection for electron and muon respectively. Data are compared with the simulations where the Z+jets events are described by MadGraph+pythia6, and good agreement is observed. In all figures, the simulated events are reweighted by scale factors in order to compensate for the residual data-to-simulation discrepancies in lepton selection efficiency, JES and JER calibration, and b tagging efficiency. The background contributions from Z+jets and $\mathrm{t\bar{t}}$ events as adjusted in Sect. 5 are included in Figs. 1 and 2.

5 Background estimation

A Drell–Yan event in which a Z boson decays into $\tau^+\tau^-$ may contribute to the dielectron or dimuon signal events if both τ leptons decay into electrons or muons. These events are treated as a background source and, being at the few per mil level, their contribution is evaluated from simulation.

The process $\mathrm{pp} \to \mathrm{t\bar{t}} \to \mathrm{W^+bW^-\bar{b}} \to \ell^+\ell^-\mathrm{b\bar{b}} + E_{\mathrm{T}}^{\mathrm{miss}}$ is the dominant non-Drell–Yan background source. The $\mathrm{t\bar{t}}$ background contribution is estimated separately for Z+jets, Z(1b), and Z(2b) events by using the signal selection criteria to produce samples of $\mathrm{e}\mu$ pairs, which are enriched in $\mathrm{t\bar{t}}$ events with negligible signal contamination. For each measured observable these samples provide the estimates of the $\mathrm{t\bar{t}}$ background; residual non-$\mathrm{t\bar{t}}$ backgrounds in them, amounting to about 29, 8 and 2% respectively, are subtracted using the simulated prediction. The integrals of such esti-

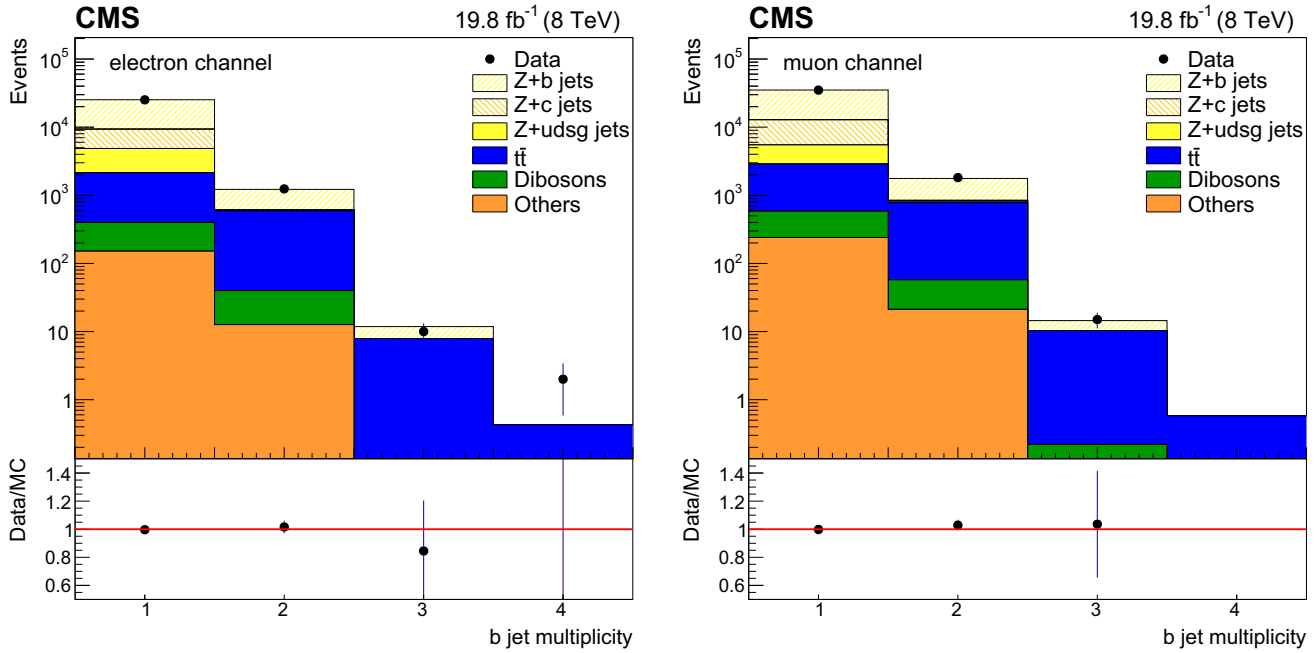

Fig. 1 Exclusive b-tagged jet multiplicity distributions for Z(1b) events, for the electron (*left*) and muon (*right*) decay channel of Z boson. *Error bars* account for statistical uncertainties in data in the *upper plots* and in both data and simulation in the *bottom ratio plots*, that show the data to MC ratio

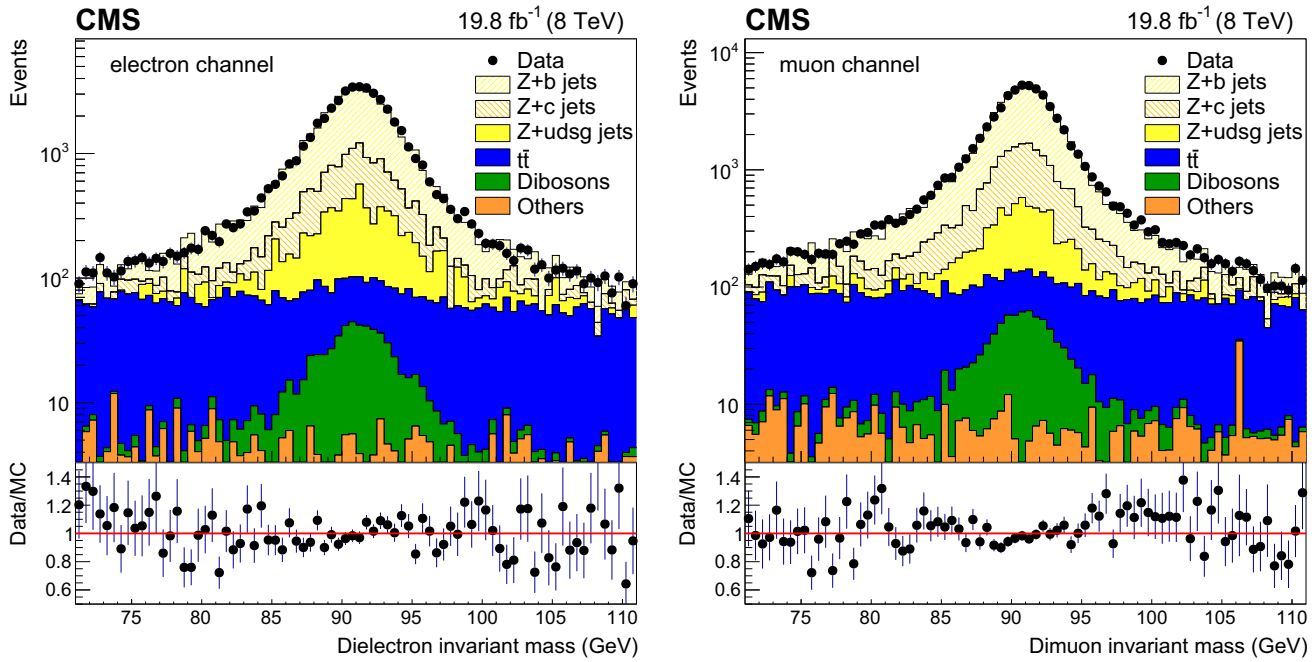

Fig. 2 Dilepton invariant mass distributions for Z(1b) events, for the electron (*left*) and muon (*right*) Z boson decay channels. *Error bars* account for statistical uncertainties in data in the *upper plots* and in both data and simulation in the *bottom ratio plots*, that show the data to MC ratio

mates need to be rescaled by the ratio of the same-flavour lepton to eμ yields. This ratio is determined using control samples for both the same-flavour lepton and eμ selections by inverting the $E_{\mathrm{T}}^{\mathrm{miss}}$ significance requirement, namely, $E_{\mathrm{T}}^{\mathrm{miss}}$ significance >30. For the same-flavour lepton samples, this selection removes the contribution from the signal processes, while enhancing the fraction of $\mathrm{t\bar{t}}$ events in the sample. The residual contamination from other non-$\mathrm{t\bar{t}}$ processes is simi-

lar in the same-lepton and eμ selections, amounting to about 20, 7, 3% respectively, and is again taken into account using the simulation. The ratio of the eμ to the ee or $\mu\mu$ yields in the control samples is used to rescale the estimates of this background source for each lepton channel separately. The ratio is determined as the scaling factor for the normalization of the binned dilepton invariant mass ($M_{\ell\ell}$) distribution in the eμ sample that minimizes the difference of this distribution from the corresponding same-lepton-flavour $M_{\ell\ell}$ distribution in a least-square fit procedure. The fit of the $M_{\ell\ell}$ distribution is performed in the sideband regions 50–84 GeV and 100–200 GeV, to avoid any assumption about the $M_{\ell\ell}$ shape for both different and same-flavour lepton pairs in the Z peak region.

The remaining background sources are estimated using simulation. Diboson events may mimic the Z+b final state when one or more leptons are not reconstructed or when a W or Z boson decays hadronically into a $\mathrm{q\bar{q}}$ pair (in particular a Z boson may decay into a genuine $\mathrm{b\bar{b}}$ pair). Single top quarks produced in association with either a W boson or one or more b jets may also generate a signal-like signature. These events, together with W+jets, can mimic the signal if a lepton of the same flavour is produced in the hadronization or if a hadron is misidentified. The contribution of multijet events is found to be negligible, as has been previously observed in other similar Z+jets analyses [45].

After subtraction of all non-Drell–Yan background contributions, the extraction of the Z(1b) and Z(2b) event yields requires an evaluation of the purity of the b tagging selection, i.e. the fraction of selected Drell–Yan events in which the desired number of b-tagged jets, at least one or at least two, originate from the hadronization of a corresponding number of b quarks. This fraction is determined from a study of the secondary vertex mass distribution of the leading b-tagged jet, defined as the invariant mass of all the charged particles associated with its secondary vertices, assuming the pion mass for each considered particle. This evaluation is done separately for dielectron and dimuon final states to avoid correlations between channels and to simplify the combination. The secondary vertex mass distributions for b, c, and light-flavour jets produced in association with Z bosons are obtained from the simulation based on the MadGraph event generator interfaced with pythia6 by using the 5FS scheme for PDFs. The sum of the distributions is fitted to the observed distribution with an extended binned likelihood, after subtraction of all non-Drell–Yan background contributions, by varying the three normalization scale factors c_b, c_c, c_udsg for the various components. The c_c, c_udsg factors are used for the subtraction of the respective components. This procedure reduces the dependence on the normalization of the b hadron production and decay in the simulation because the expected shape of the secondary vertex mass distribution is used. In the case of the Z(2b) selection, as it can be seen in Fig. 1, the contamination from c and light-flavour jets is negligible and is subtracted using simulation; only the c_bb scaling factor for the genuine double b jet component is determined from the fit, and it is used only to correct the relative proportion of Z(1b) and Z(2b) events in the simulation, as discussed in Sect. 6.

The results of the fit to the secondary vertex mass distributions are presented in Fig. 3 for the Z(1b) analysis, showing the flavour composition in each channel. Data-to-simulation scale factors, as determined by the fit, are given in Table 1 for both event selections and Z boson decay channels. The flavour composition of the selected sample after the scale factor corrections for the Z(1b) samples is also shown.

The b-flavour contribution is constrained by the high secondary vertex mass region of the distribution of the CSV discriminating variable, while the c-flavour contribution is mostly important in the region between 1 and 2 GeV, and the light-flavour contribution below 1 GeV. This results in a strong anticorrelation both between the b- and c-flavour and between c- and light-flavour contributions, with an estimated correlation coefficient of about -0.6 in both cases, whereas the correlation between the b- and light-flavour contributions is negligible. As a consequence, a fluctuation in the small c quark component may cause a difference in the scale factors between different lepton channels.

The signal yield for Z(1b) events is therefore obtained, for each bin of a distribution, from the selected event yield N^{selected} as

$$N_{\mathrm{Z(1b)}} = N^{\text{selected}}_{\mathrm{Z(1b)}} - N_{\mathrm{t\bar{t}}} - N^{\mathrm{MC}}_{\mathrm{Dibosons}} - N^{\mathrm{MC}}_{\mathrm{Others}} - c_\mathrm{c} N^{\mathrm{MC}}_{\mathrm{Z+c}} - c_\mathrm{udsg} N^{\mathrm{MC}}_{\mathrm{Z+udsg}},$$

where $N_{\mathrm{t\bar{t}}}$, $N^{\mathrm{MC}}_{\mathrm{Dibosons}}$, and $N^{\mathrm{MC}}_{\mathrm{Others}}$ are the $\mathrm{t\bar{t}}$, diboson, and other background contributions respectively, $c_\mathrm{c} N^{\mathrm{MC}}_{\mathrm{Z+c}}$ and $c_\mathrm{udsg} N^{\mathrm{MC}}_{\mathrm{Z+udsg}}$ are the numbers of Drell–Yan events in which the b-tagged jets originate from either a c or a light-flavour parton, and the scale factors multiply the event yields predicted by the simulation. For the calculation of the Z(2b) event yield a similar procedure is applied:

$$N_{\mathrm{Z(2b)}} = N^{\text{selected}}_{\mathrm{Z(2b)}} - N_{\mathrm{t\bar{t}}} - N^{\mathrm{MC}}_{\mathrm{Dibosons}} - N^{\mathrm{MC}}_{\mathrm{Others}}.$$

The c_c and c_udsg scale factors are also re-evaluated from subsamples obtained by dividing the ranges of the studied observables into wide intervals, in order to study a possible correlation with the observables themselves. The statistical uncertainty of these scale factors depends on the chosen observable and binning, ranging from a factor of 2 up to 10 relative to the size of the uncertainty of the default values obtained with the full sample. Because no statistically significant dependence is observed, the scale factors estimated from the overall sample are used.

The amount of background in the final event selection, estimated with the procedures discussed above, can be

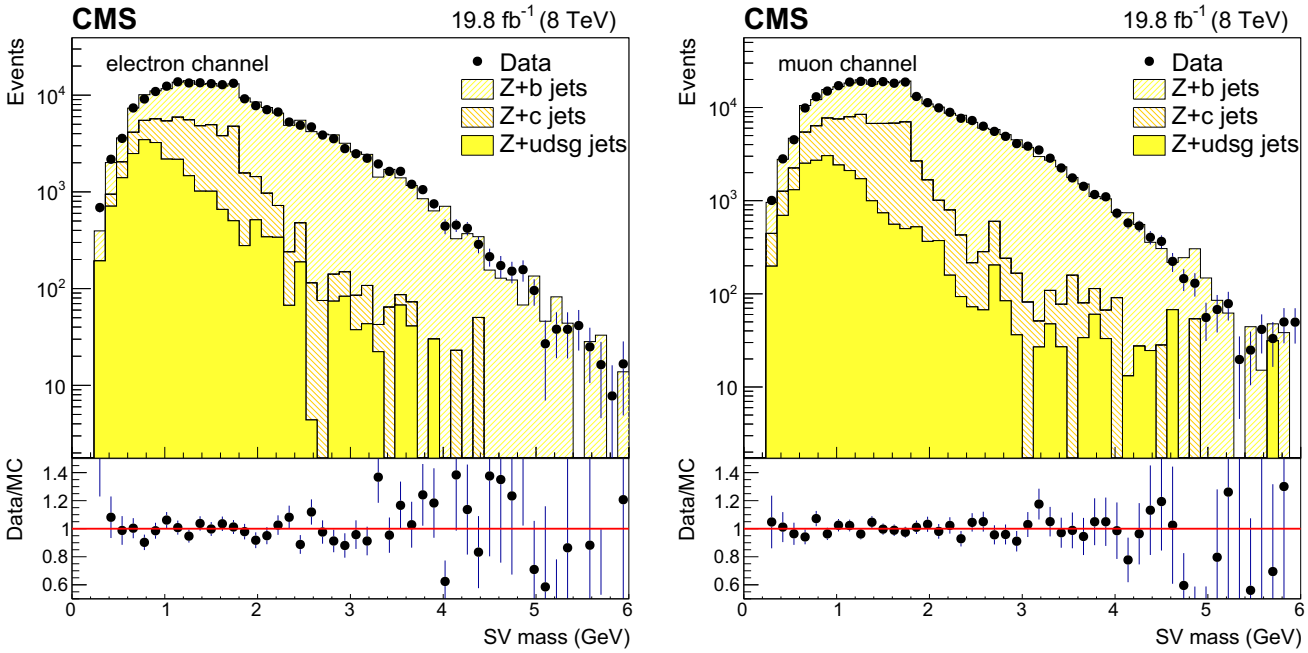

Fig. 3 Distributions of the secondary vertex (SV) mass of the leading jet after the Z(1b) selection with the Z boson decaying into electrons (*left*) and muons (*right*). The subsamples corresponding to b-tagged jets originating from b, c, and light-flavour quarks or gluons are shown, with normalizations determined in the fit to data. Non-Drell–Yan background sources are subtracted. *Error bars* account for statistical uncertainties in data in the *upper plots* and in both data and simulation in the *bottom ratio plots*

Table 1 Normalization scale factors and post-fit fractions for b, c and light-flavour (u, d, s quark and gluon) components in the selected Z(1b) events, and scale factor for b in the selected Z(2b) events, obtained from a fit to the secondary vertex mass distribution for dielectron and dimuon final states. The quoted uncertainties are statistical only

Event selection	c_b	c_c	c_{udsg}	Z(1b) (%)	Z+c (%)	Z+udsg (%)
Z(1b) (ee)	0.91 ± 0.02	1.29 ± 0.13	1.70 ± 0.21	69.5 ± 1.8	19.0 ± 2.0	11.4 ± 1.4
Z(1b) ($\mu\mu$)	0.91 ± 0.02	1.51 ± 0.12	1.18 ± 0.19	69.7 ± 1.5	22.4 ± 1.8	7.9 ± 1.2

Event selection	c_{bb}
Z(2b) (ee)	1.18 ± 0.12
Z(2b) ($\mu\mu$)	1.17 ± 0.09

observed in Fig. 1. For the Z(1b) selection, in the electrons (muons) samples the Z+c contribution amounts to about 17% (20%), the Z+light flavour jets (including gluons) to 10% (7%), and the $t\bar{t}$ to 9% (8%). Other background contributions are globally below the 2% level. The Z(1b) contribution in the corresponding selected sample is about 62% (63%) for the electrons (muons) channel.

6 Unfolding

The differential event yields are corrected for event selection efficiencies and for detector resolution effects back to the stable-particle level. For this purpose, the singular value decomposition (SVD) [46] unfolding technique, implemented in the RooUnfold toolkit [47], is used. The unfolding procedure is based on a response matrix, which describes the relationship between the particle levels and measured values of a given observable due to the detector resolution and acceptance. The response matrix is calculated using Z(1b) events that are generated with MadGraph in the 5FS, interfaced to pythia6, and followed by the detector simulation. Response matrices are computed separately for the Z(1b) and Z(2b) selections. The proportion of events with exactly one or at least two b quarks in the simulation is reweighted to match that observed in data, as determined by the c_{bb} scaling factor.

Fiducial cross sections are defined, based on event generator predictions at the particle level, for leptons and jets reconstructed from the collection of all stable final-state par-

ticles, using the same selection criteria as the data analysis. The two leptons (electrons or muons) with the highest transverse momentum and with $p_T > 20$ GeV and $|\eta| < 2.4$ are selected as Z boson decay products if their invariant mass is in the range of 71–111 GeV. Electromagnetic final-state radiation effects are taken into account in the generator-level lepton definition by clustering all photons in a cone of radius $\Delta R = 0.1$ around the final-state leptons. The leptons selected as Z boson decay products are then removed from the particle collection used for the jet clustering at the generator level. The remaining particles, excluding neutrinos, are clustered into jets using the anti-k_t algorithm with a distance parameter of 0.5. Generated jets are selected if their distance from the leptons forming the Z boson candidate is larger than $\Delta R = 0.5$. Jets originating from the hadronization of b quarks are selected if a b hadron is an ancestor of one of the particles clustered in it, and this b hadron has a distance from the jet in the η-ϕ plane of $\Delta R \leq 0.5$. Jets and b jets are selected if they have $p_T > 30$ GeV and lie in the pseudorapidity range $|\eta| < 2.4$.

As a cross-check of the SVD technique, the unfolding is also performed with the iterative D'Agostini method [48], leading to compatible results within the statistical uncertainties.

7 Systematic uncertainties

Several sources of systematic uncertainty affect the cross section measurement: the JES and JER, the calculation of the unfolding response matrix, the estimation of the b quark fraction, the background subtraction, the event selection efficiencies, the pileup description, and the integrated luminosity. For every source other than the luminosity, the full analysis procedure is repeated after the variation of the corresponding input values, and the difference of the extracted cross section with respect to the central measurement is used as an estimate of the uncertainty due to that source. The uncertainties are symmetrized, if not already symmetric. The systematic uncertainties in the measured Z(1b) and Z(2b) differential cross sections are summarized in Table 2 and in Tables 3 and 4, respectively.

Reconstructed jet energies must be corrected for several effects, such as pileup contamination, instrumental noise, nonuniformities and nonlinearities in the detector response, and flavour composition. The resulting uncertainty depends on the transverse momentum and pseudorapidity of the jet. The systematic effect due to the application of JES corrections in the data is estimated by increasing and decreasing the correction parameters deviation from their nominal values by one standard deviation. The uncertainty for the JER correction is evaluated in the same way.

For the cross section measurement in a given bin, the systematic uncertainty induced by the model used in the unfolding procedure is evaluated as the difference between the standard result and that obtained with an alternative model for unfolding, namely MadGraph5_aMC@NLO interfaced with pythia8. This alternative model implements NLO hard scattering matrix elements, compared to the LO matrix elements of MadGraph interfaced to pythia6, and also includes different details of the underlying event, hadronization, and particle decay descriptions compared to the default choice. In order to evaluate the genuine model-induced effects, the statistical uncertainties from the two simulated samples are subtracted in quadrature from the difference; any negative results so obtained are replaced with zero. The uncertainty associated with the size of the simulated sample used to compute the response matrix elements is determined by producing replicas of the matrix whose elements are fluctuated according to a Poisson distribution.

The uncertainty induced by the secondary vertex mass fit, used to extract the true flavour composition of the Z(1b) sample, is twofold. One part is due to the statistical uncertainty in the c_c, c_{udsg} scale factors, whose effect is estimated by varying them up and down by one standard deviation, taking into account their correlation. This source of uncertainty is considered as part of the statistical uncertainty, because it is due to the finite size of the collision data sample. The other part stems from the choice of the simulation model for the shape of the secondary vertex mass distributions. This choice affects also the correction of the relative proportion of different b multiplicities provided by the scale factor c_{bb}. In addition, a systematic uncertainty is associated, for both Z(1b) and Z(2b) samples, with the modelling of the c quark and light-flavour contributions to each measured observable. Both of these model-induced uncertainties, collectively indicated in the tables as "c, udsg background model", are estimated by replacing the default model given by MadGraph 5FS interfaced with pythia6 with MadGraph5_aMC@NLO 5FS interfaced with pythia8. The scale factors, which are determined from the alternative model, are in statistical agreement for dielectron and dimuon channels within one standard deviation. The difference between the results obtained with the two models is therefore considered as safely accounting for possible residual discrepancies between data and simulation.

For each lepton channel the systematic uncertainties in the lepton efficiency calculations for triggering, reconstruction, identification, and isolation are estimated from the $Z \to \ell\ell$ "tag-and-probe" measurements of data-to-simulation efficiency scale factors. The global effect of the systematic uncertainty related to the scale factors is 1.5% in the dielectron final state and 2% in the dimuon final state. The uncertainties in the b tagging efficiency scale factors include contributions from the pileup contamination, the gluon splitting rate in simulation ($g \to b\bar{b}$), varied by $\pm 50\%$, and the energy

Table 2 Uncertainties (in percent) in the differential cross sections as a function of the leading b jet p_T and $|\eta|$, the Z boson p_T, H_T, and $\Delta\phi_{Zb}$ between the Z boson and the leading b jet, for the Z(1b) sample

Uncertainty (%)	$d\sigma/dp_T$	$d\sigma/d\lvert\eta\rvert$	$d\sigma/dp_T^Z$	$d\sigma/dH_T$	$d\sigma/d\Delta\phi_{Zb}$
JER	0.3–1.7	0.1–0.6	0.2–2.6	0.4–1.9	0.1–2.2
JES	0.5–4.8	0.7–5.3	0.5–7.7	0.6–5.2	0.4–4.2
Unfolding (MC model)	0.0–19.2	0.2–2.2	0.0–18.1	0.0–10.2	0.0–9.2
Unfolding (MC statistics)	1.4–10.2	1.1–2.7	1.8–8.3	1.3–7.6	1.2–6.1
c, udsg background model	0.0–6.1	0.0–7.0	0.0–19.9	0.7–7.5	0.0–10.9
Electron (muon) efficiency	1.5 (2.0)	1.5 (2.0)	1.5 (2.0)	1.5 (2.0)	1.5 (2.0)
b tagging efficiency	3.0	3.0	3.0	3.0	3.0
Pileup	0.2–4.3	0.6–1.4	0.4–2.0	0.2–2.3	0.2–1.6
Background (systematic)	0.1–0.4	0.1–0.3	0.1–0.6	0.2–0.3	0.1–0.3
Background (statistical)	1.2–7.2	1.0–2.5	1.5–5.8	1.3–4.6	1.2–5.9
Integrated luminosity	2.6	2.6	2.6	2.6	2.6
Total syst. uncertainty (%)	5.5–21.7	5.2–10.6	5.6–22.8	8.4–13.8	6.0–13.3
Total stat. uncertainty (%)	2.6–8.8	3.0–5.4	2.9–8.6	3.1–6.0	3.1–7.0

Table 3 Uncertainties (in percent) in the differential cross sections as a function of the leading and subleading b jet p_T, the Z boson p_T, the invariant mass of the two b-tagged jets, and the invariant mass of the Z boson and the two b-tagged jets, for the Z(2b) sample

Uncertainty (%)	$d\sigma/dp_T^{leading}$	$d\sigma/dp_T^{subleading}$	$d\sigma/dp_T^Z$	$d\sigma/dM_{bb}$	$d\sigma/dM_{Zbb}$
JER	0.3–8.3	0.7–7.9	0.1–3.8	0.9–4.1	2.9–12.0
JES	4.4–17.0	7.7–23.3	3.1–20.3	6.7–15.3	3.8–16.2
Unfolding (MC model)	0.0–74.4	0.0–52.6	0.0–53.6	0.0–37.8	0.0–57.3
Unfolding (MC statistics)	8.0–39.4	9.0–35.8	8.8–27.0	7.6–28.0	10.0–20.8
c, udsg background model	0.0–17.3	0.0–16.1	0.0–15.5	0.0–18.5	0.0–10.2
Electron (muon) efficiency	1.5 (2.0)	1.5 (2.0)	1.5 (2.0)	1.5 (2.0)	1.5 (2.0)
b tagging efficiency	6.0	6.0	6.0	6.0	6.0
Pileup	0.4–14.1	0.3–11.4	1.3–9.6	1.1–5.7	0.2–4.3
Background (systematic)	0.3–0.9	0.1–0.7	0.3–1.2	0.0–1.4	0.3–1.3
Background (statistical)	3.1–17.4	4.0–24.2	4.2–15.0	4.3–15.0	5.8–10.2
Integrated luminosity	2.6	2.6	2.6	2.6	2.6
Total syst. uncertainty (%)	17.2–89.4	19.7–61.7	17.8–56.6	14.5–52.9	17.9–65.4
Total stat. uncertainty (%)	6.1–34.1	7.6–44.5	10.4–23.5	7.9–28.0	11.2–19.9

Table 4 Uncertainties (in percent) in the differential cross sections as a function of ΔR and $\Delta\phi$ between the two b-tagged jets, ΔR between the Z boson and the closer b-tagged jet, and the asymmetry A_{Zbb}, for the Z(2b) sample

Uncertainty (%)	$d\sigma/d\Delta\phi_{bb}$	$d\sigma/d\Delta R_{bb}$	$d\sigma/d\Delta R_{Zb}^{min}$	$d\sigma/dA_{Zbb}$
JER	0.8–2.0	1.0–5.3	0.6–6.1	0.6–4.2
JES	5.6–10.7	6.6–20.5	4.2–13.1	5.1–9.1
Unfolding (MC model)	0.0–47.0	0.0–206	0.0–50.6	2.6–33.1
Unfolding (MC statistics)	6.3–11.5	6.4–30.7	8.2–25.6	7.5–30.5
c, udsg background model	0.0–3.4	0.0–10.3	0.0–14.2	0.0–12.3
Electron (muon) efficiency	1.5 (2.0)	1.5 (2.0)	1.5 (2.0)	1.5 (2.0)
b tagging efficiency	6.0	6.0	6.0	6.0
Pileup	0.4–2.4	1.3–3.5	0.5–4.6	1.2–6.1
Background (systematic)	0.1–0.8	0.1–0.8	0.2–1.3	0.2–0.7
Background (statistical)	3.4–5.0	3.7–9.4	3.6–15.9	3.3–8.8
Integrated luminosity	2.6	2.6	2.6	2.6
Total syst. uncertainty (%)	13.0–50.5	12.5–209	14.2–59.5	13.6–47.2
Total stat. uncertainty (%)	6.9–10.1	7.5–17.6	7.4–33.1	6.6–18.4

fraction carried by the b hadrons in the hadronization (varied by ±5%) [42]. The global value of the b tagging systematic uncertainty amounts to 3% per b-tagged jet. Scale factors for c jets, assumed equal to those for b jets, are assigned an uncertainty twice as large as for the b jets.

The simulation is reweighted according to the generated primary vertex multiplicity and the instantaneous luminosity in data to reproduce the observed primary vertex multiplicity distribution, and provide a reliable representation of pileup. The minimum-bias event cross section in simulation is tuned to provide the best agreement between data and simulation in the vertex multiplicity distribution of $Z \to \mu\mu$ events. The uncertainty associated with this procedure is estimated by varying this minimum-bias cross section value by 5%.

The uncertainty in the $t\bar{t}$ background normalization is derived from the statistical uncertainties of the same-flavour and $e\mu$ control samples and is included in the total statistical uncertainty. The systematic uncertainty related to the diboson background (ZZ, WW, WZ) is evaluated by varying the theoretical production cross sections by ±15% of their central values, corresponding to about three standard deviations of the overall theoretical normalization uncertainty and covering the typical differences between the theoretical and measured values. In addition, the statistical uncertainty induced by the limited size of simulation samples is taken into account.

The systematic uncertainty in the integrated luminosity is 2.6% [49].

In the ratios of Z(1b) and Z(2b) to the inclusive Z+jets cross sections, the uncertainties are simultaneously propagated to both the numerator and denominator, taking correlations into account. The uncertainties in the energy scale, resolution, and efficiency corrections for reconstructed leptons and jets are considered to be fully correlated, as is the uncertainty in the integrated luminosity. Tables 2, 3 and 4 summarize the ranges of variation of the uncertainties for each observable measured with the Z(1b) and Z(2b) samples.

8 Results and comparison with theoretical predictions

8.1 Observables

Differential cross sections as a function of a number of kinematic observables are measured in order to characterize the production mechanisms of Z(1b) events.

For Z(1b) events, five kinematic observables are studied. First, p_T and $|\eta|$ of the leading-p_T b jet are measured, together with the Z boson p_T. The distributions of these variables are directly sensitive to the b quark PDF and initial-state gluon splitting and may show differences between different PDF flavour schemes. Searches for physics processes beyond the SM in Lorentz-boosted topology events depend on precise knowledge of the Z boson p_T distribution. The scalar sum H_T of the transverse momenta of all selected jets, regardless of their flavour, is related to the structure of the hadronic system recoiling against the boson. The measurement of this observable at high values is potentially sensitive to the presence of intermediate heavy particles decaying hadronically, as predicted, for example, in some SUSY scenarios. Finally, the topology of the system composed of the Z boson and b jet is studied by measuring the cross section as a function of the azimuthal angular separation between the direction of the Z boson and the direction of the highest-p_T b jet, $\Delta\phi_{Zb}$. This observable is also sensitive to the presence of boosted particles decaying into a Z boson and b quarks.

Ratios of the differential cross sections for Z(1b) and Z+jets events, inclusive in the jet flavour, are also measured:

$$R(x) = \frac{\mathrm{d}\sigma(\mathrm{Z}+(\geq 1\mathrm{b}))/\mathrm{d}x}{\mathrm{d}\sigma(\mathrm{Z}+\mathrm{jets})/\mathrm{d}x},$$

with x representing one of the five observables described above. The inclusive Z+jets event selection is defined by releasing the requirement of a b-tagged jet in the Z(1b) selection. In these ratios the kinematic observables referring to the highest-p_T b-tagged jet from the Z(1b) sample are used in the numerator, while for the denominator the observables related to the highest-p_T jet from the Z+jet sample are examined. Several systematic uncertainties cancel in the ratios, allowing a precise comparison with theory.

For Z(2b) events, the cross section is measured as a function of the transverse momenta of the Z boson and of the leading and subleading b jets. In addition, the cross section is studied as a function of several variables explicitly related to the topology of the final state consisting of a Z boson and the two highest-p_T b jets. The invariant mass M_{bb} of the bb system and the invariant mass M_{Zbb} of the Zbb system are studied, because their distributions are sensitive to the presence of heavy intermediate particles.

Angular correlations between the b jets and between each b jet and the Z boson are described by four observables, also studied in Ref. [9]. The azimuthal angular separation $\Delta\phi_{bb}$ between the directions of the two b jets in the transverse plane is useful to identify back-to-back configurations of the b quarks. The distance between the directions of the two b jets in the η-ϕ plane is defined as $\Delta R_{bb} = \sqrt{(\Delta\eta_{bb})^2 + (\Delta\phi_{bb})^2}$, where $\Delta\eta_{bb}$ is the separation in pseudorapidity between the two b jets. This variable is sensitive to the different production mechanisms of the Z(2b) final-state b quarks. In particular, it is useful to discriminate between the contributions whose scattering amplitudes are dominated by terms involving gluon splitting, $g \to b\bar{b}$, and those where a Z boson is emitted from one of the final-state b quarks. The process $q\bar{q} \to Zb\bar{b}$ contributes to both cases, while $qg \to Zb\bar{b}X$ (with X an additional parton) contributes to the former and

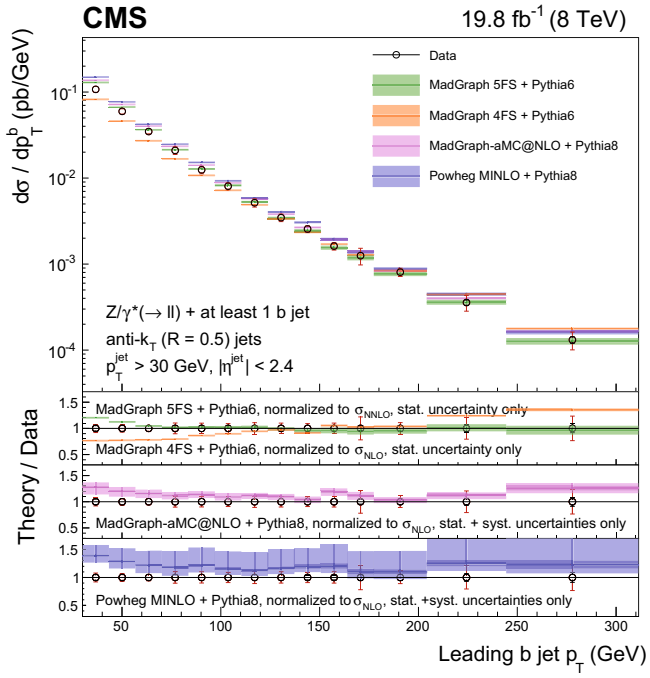

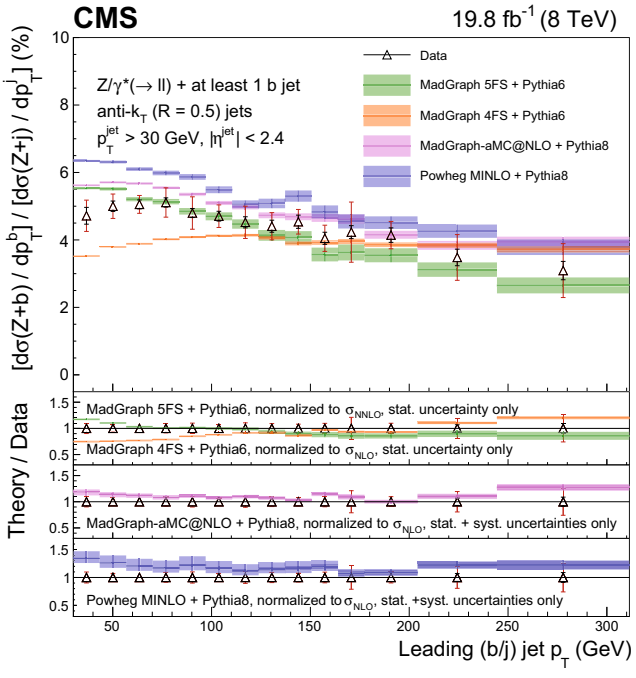

Fig. 4 Differential fiducial cross section for Z(1b) production as a function of the leading b jet p_T (*left*), and the cross section ratio for Z(1b) and Z+jets production as a function of the leading b/inclusive (j) jet p_T (*right*), compared with the MADGRAPH 5FS, MADGRAPH 4FS, MADGRAPH5_aMC@NLO, and POWHEG MINLO theoretical predictions (*shaded bands*), normalized to the theoretical cross sections described in the text. For each data point the statistical and the total (sum in quadrature of statistical and systematic) uncertainties are represented by the *double error bar*. The width of the *shaded bands* represents the uncertainty in the theoretical predictions, and, for NLO calculations, the *inner darker area* represents the statistical component only

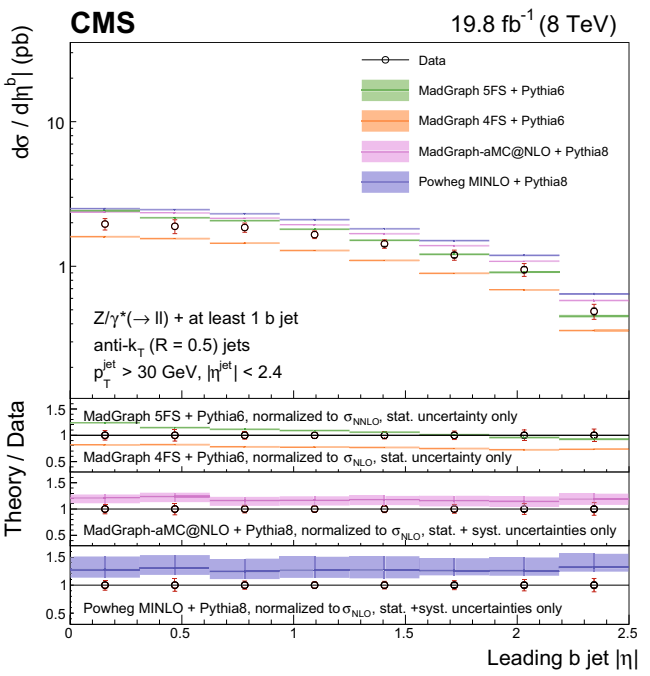

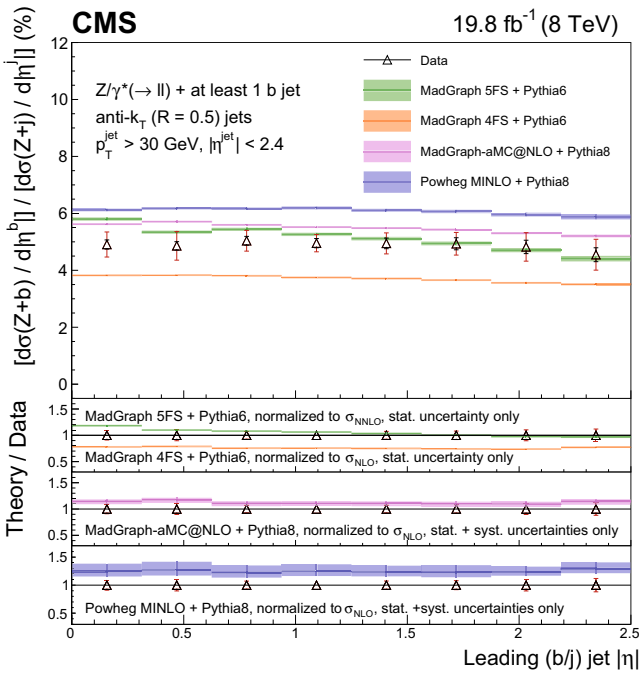

Fig. 5 Differential fiducial cross section for Z(1b) production as a function of the leading b jet $|\eta|$ (*left*), and the cross section ratio for Z(1b) and Z+jets production as a function of the leading b/inclusive (j) jet $|\eta|$ (*right*), compared with the MADGRAPH 5FS, MADGRAPH 4FS, MADGRAPH5_aMC@NLO, and POWHEG MINLO theoretical predictions (*shaded bands*), normalized to the theoretical cross sections described in the text. For each data point the statistical and the total (sum in quadrature of statistical and systematic) uncertainties are represented by the *double error bar*. The width of the *shaded bands* represents the uncertainty in the theoretical predictions, and, for NLO calculations, theoretical systematic uncertainties are added in the ratio plots with the *inner darker area* representing the statistical component only

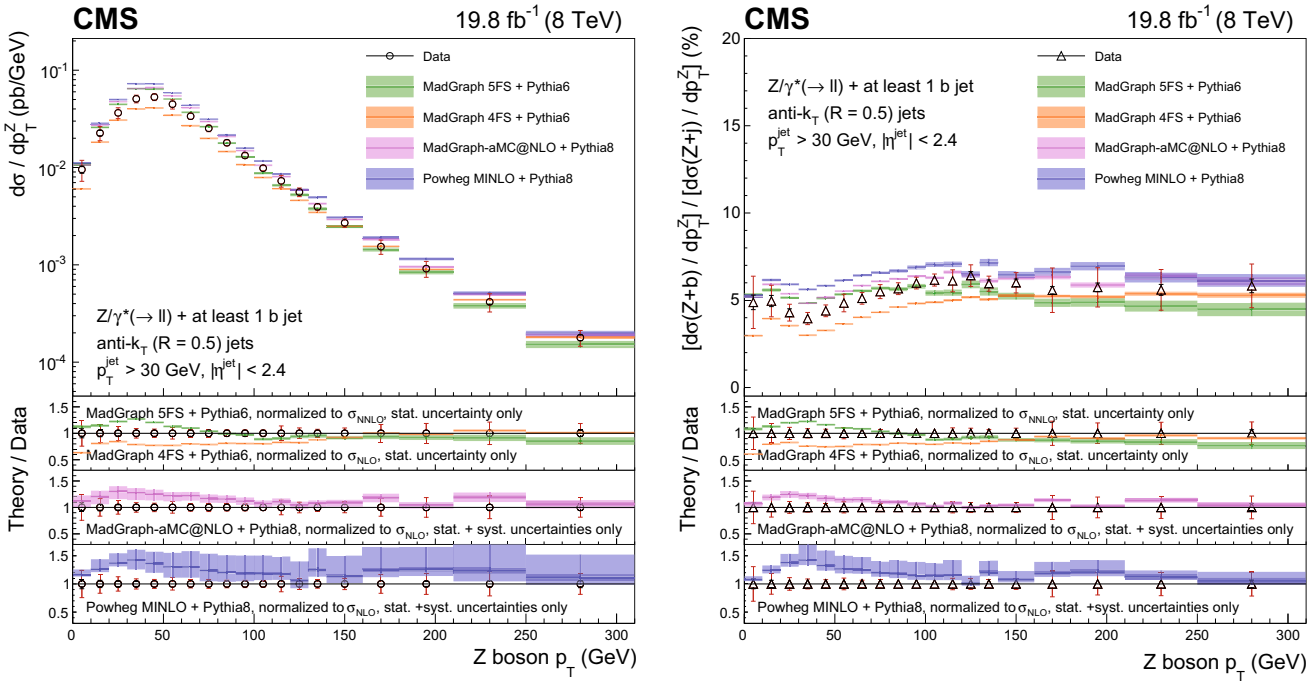

Fig. 6 Differential fiducial cross section for Z(1b) production as a function of the Z boson p_T (*left*), and the cross section ratio for Z(1b) and Z+jets production as a function of the Z boson p_T (*right*), compared with the MADGRAPH 5FS, MADGRAPH 4FS, MADGRAPH5_aMC@NLO, and POWHEG MINLO theoretical predictions (*shaded bands*), normalized to the theoretical cross sections described in the text. For each data point the statistical and the total (sum in quadrature of statistical and systematic) uncertainties are represented by the *double error bar*. The width of the *shaded bands* represents the uncertainty in the theoretical predictions, and, for NLO calculations, theoretical systematic uncertainties are added in the ratio plots with the *inner darker area* representing the statistical component only

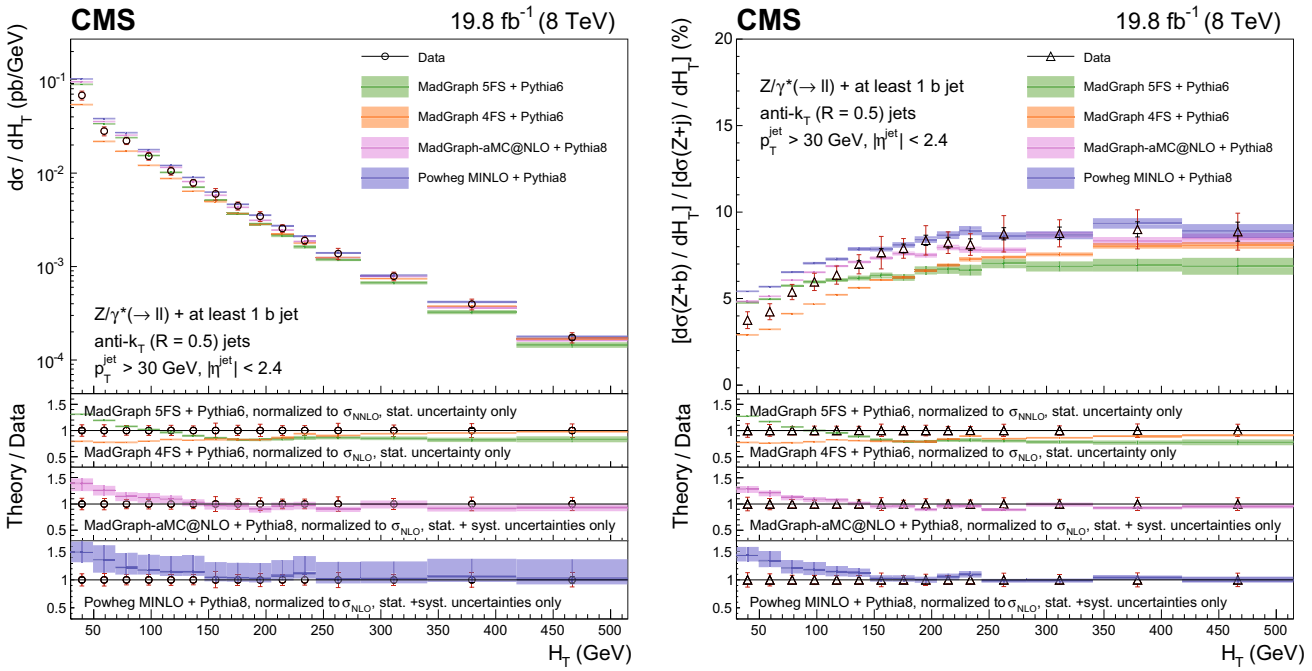

Fig. 7 Differential fiducial cross section for Z(1b) production as a function of H_T (*left*), and the cross section ratio for Z(1b) and Z+jets production as a function of H_T (*right*), compared with the MADGRAPH 5FS, MADGRAPH 4FS, MADGRAPH5_aMC@NLO, and POWHEG MINLO theoretical predictions (*shaded bands*), normalized to the theoretical cross sections described in the text. For each data point the statistical and the total (sum in quadrature of statistical and systematic) uncertainties are represented by the *double error bar*. The width of the *shaded bands* represents the uncertainty in the theoretical predictions, and, for NLO calculations, theoretical systematic uncertainties are added in the ratio plots with the inner darker area representing the statistical component only

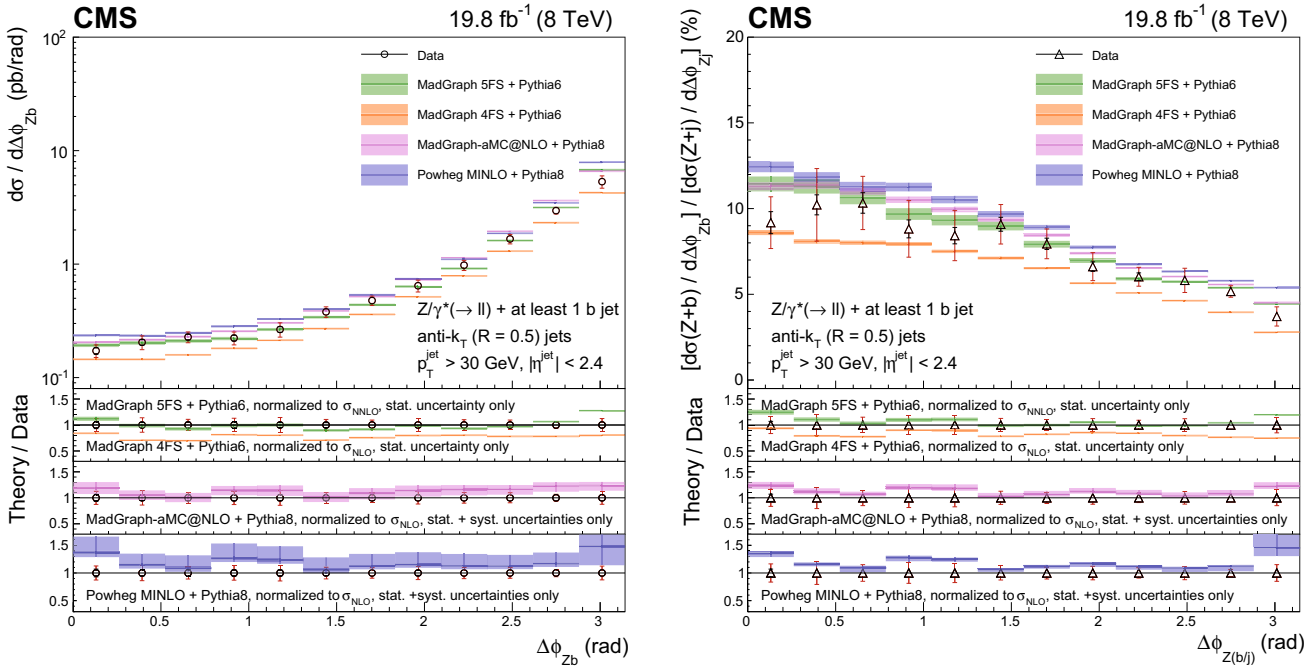

Fig. 8 Differential fiducial cross section for Z(1b) production as a function of $\Delta\phi_{\mathrm{Zb}}$ (*left*), and the cross section ratio for Z(1b) and Z+jets production as a function of $\Delta\phi_{\mathrm{Z(b/j)}}$ (*right*), compared with the MADGRAPH 5FS, MADGRAPH 4FS, MADGRAPH5_aMC@NLO, and POWHEG MINLO theoretical predictions (*shaded bands*), normalized to the theoretical cross sections described in the text. For each data point the statistical and the total (sum in quadrature of statistical and systematic) uncertainties are represented by the *double error bar*. The width of the *shaded bands* represents the uncertainty in the theoretical predictions, and, for NLO calculations, theoretical systematic uncertainties are added in the ratio plots with the *inner darker area* representing the statistical component only

$\mathrm{gg} \rightarrow \mathrm{Zb\bar{b}}$ to the latter. These contributions correspond, respectively, to the regions where the two b quarks are almost collinear or mostly acollinear. Because two b jets must be reconstructed, this measurement cannot be sensitive to low-angle gluon splitting, where the distance between the jet-initiating partons is smaller than twice the jet size. This region is better explored by searching directly for pairs of b hadrons close in space, as studied in Ref. [9], whose decay products might be part of a single reconstructed jet. Another angular observable of interest is $\Delta R_{\mathrm{Zb}}^{\mathrm{min}}$, the angular separation between the Z boson and the closer b jet in the η–ϕ plane. This variable is useful for testing multileg tree-level and NLO corrections in which a Z boson is radiated from a quark, because it is sensitive to event topologies with the Z boson in the vicinity of one of the two b jets. Finally, the A_{Zbb} asymmetry between the b jet direction and the Z boson direction is computed using a combination of $\Delta R_{\mathrm{Zb}}^{\mathrm{min}}$ and $\Delta R_{\mathrm{Zb}}^{\mathrm{max}}$ (the latter being the η–ϕ separation between the Z boson and the farther b jet):

$$A_{\mathrm{Zbb}} = \frac{\Delta R_{\mathrm{Zb}}^{\mathrm{max}} - \Delta R_{\mathrm{Zb}}^{\mathrm{min}}}{\Delta R_{\mathrm{Zb}}^{\mathrm{max}} + \Delta R_{\mathrm{Zb}}^{\mathrm{min}}}.$$

The A_{Zbb} asymmetry can provide an indirect test of pQCD validity at higher orders of the perturbative series. A nonzero value of A_{Zbb} is related to the emission of additional gluon radiation in the final state, while values of A_{Zbb} close to zero identify configurations in which the two b jets are emitted symmetrically with respect to the Z boson direction.

8.2 Theoretical predictions

The measured differential cross sections for the associated production of Z bosons and b jets are compared to several perturbative QCD theoretical calculations.

In pQCD the amplitude for this process can be computed using two alternative approaches. In the four-flavour scheme (4FS) [50], the b quark mass is explicitly included in the predictions and acts as an infrared cutoff, partly removing possible divergences in the matrix element calculation. This approach corresponds to an effective QCD theory, with $n_f = 4$ quark flavours involved in the computation of the running of the strong coupling constant α_S. In this scheme no b quark PDF is used, and the b quark is always produced explicitly by the gluon splitting $\mathrm{g} \rightarrow \mathrm{b\bar{b}}$ process. In the 5FS [51] (where $n_f = 5$), the gluon splitting contribution is included within the b quark PDF, and the b quark mass is set to zero in the matrix element calculation. The two schemes can be defined in such a way as to provide identical results

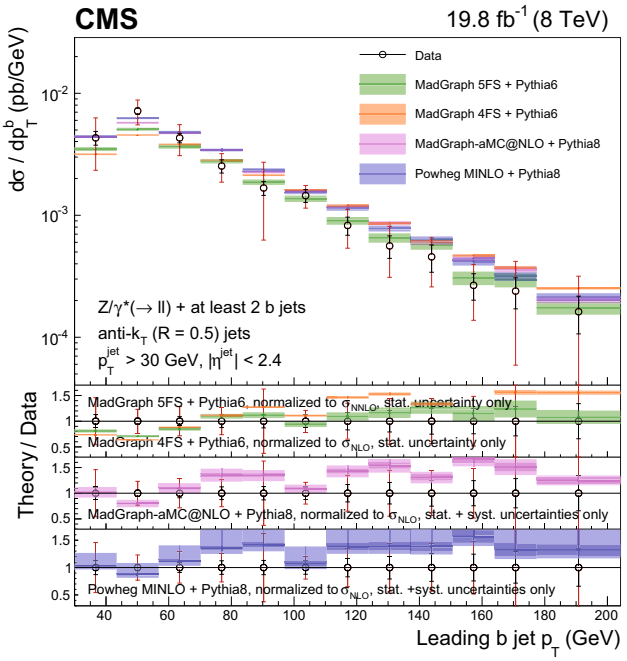

Fig. 9 Differential fiducial cross section for Z(2b) production as a function of the leading b jet p_T, compared with the MADGRAPH 5FS, MADGRAPH 4FS, MADGRAPH5_aMC@NLO, and POWHEG MINLO theoretical predictions (*shaded bands*), normalized to the theoretical cross sections described in the text. For each data point the statistical and the total (sum in quadrature of statistical and systematic) uncertainties are represented by the *double error bar*. The width of the *shaded bands* represents the uncertainty in the theoretical predictions, and, for NLO calculations, theoretical systematic uncertainties are added in the ratio plots with the *inner darker area* representing the statistical component only

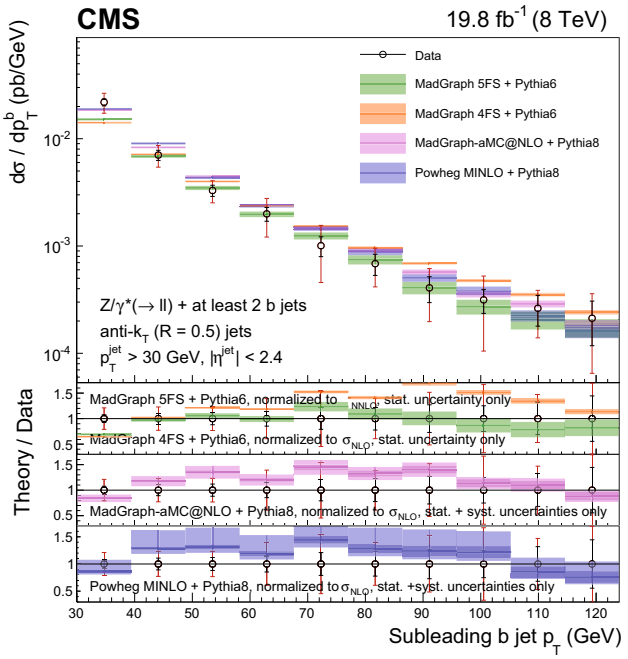

Fig. 10 Differential fiducial cross section for Z(2b) production as a function of the subleading b jet p_T, compared with the MADGRAPH 5FS, MADGRAPH 4FS, MADGRAPH5_aMC@NLO, and POWHEG MINLO theoretical predictions (*shaded bands*), normalized to the theoretical cross sections described in the text. For each data point the statistical and the total (sum in quadrature of statistical and systematic) uncertainties are represented by the *double error bar*. The width of the *shaded bands* represents the uncertainty in the theoretical predictions, and, for NLO calculations, theoretical systematic uncertainties are added in the ratio plots with the *inner darker area* representing the statistical component only

when all orders in pQCD are computed. However, differences appear in fixed-order predictions, where the different ordering of terms in the matrix element expansion gives different results. The comparison of different flavour schemes is interesting because, in pQCD, the evolution of the b quark PDF as a function of the Bjorken x variable shows sizeable differences between tree-level calculations and those at NLO. These differences are introduced by singularities in the Altarelli–Parisi splitting functions that are present only at NLO; they have no impact on the tree-level evolution of the b quark PDF [52].

While NLO calculations are now available for both flavour schemes, LO calculations are still interesting to study because they allow the inclusion of multiple additional light, hard partons in the matrix element. This feature is expected to provide a better description of the real hard radiation, compared to fixed-order NLO calculations matched with parton showering.

The MADGRAPH plus PYTHIA6 event generator, introduced in Sect. 3, describes signal events at full detector simulation level and provides theoretical predictions at tree level for the associated production of Z bosons and jets, including b jets. This calculation is based on the 5FS using the LO MADGRAPH 5.1.3.30 matrix element generator, with up to four additional partons in the matrix element calculation. The factorization and renormalization scales are chosen on an event-by-event basis as the transverse mass of the event, clustered with the k_t algorithm down to a 2→2 topology, and k_t computed at each vertex splitting, respectively [19,53]. The matrix element calculation is interfaced with PYTHIA version 6.424, using tune Z2* for parton showering, hadronization, and description of MPI. The CTEQ6L1 PDF is adopted in the calculations. The Drell–Yan inclusive cross section is rescaled to the NNLO calculation provided by FEWZ 3.1 [20,21], which has a uncertainty of about 5%. This uncertainty is not propagated into the figures presented below.

Theoretical predictions at tree level based on MADGRAPH matrix elements for the Z + 2b process are also computed using the 4FS MSTW2008 LO PDF set [54]. The factorization and renormalization scales are defined as in the 5FS case. Also in this case, parton showering and hadronization are provided by PYTHIA6 with the tune Z2*. The inclusive cross section is rescaled to the Z + 2b NLO calculation

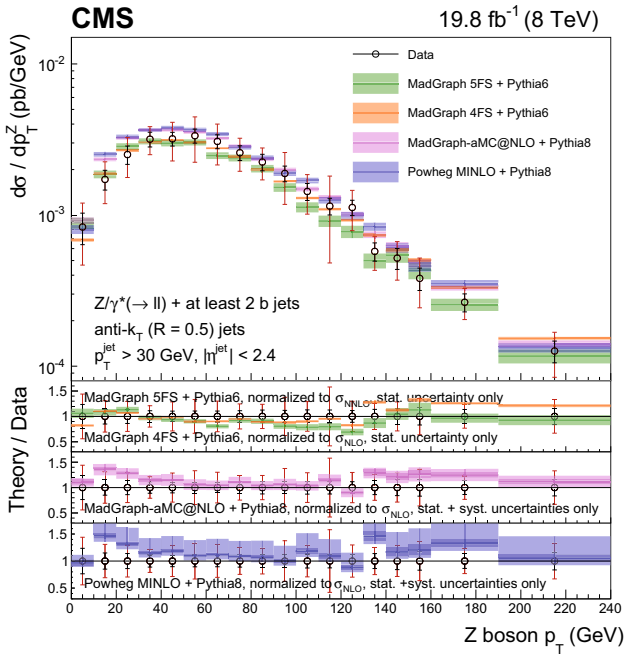

Fig. 11 Differential fiducial cross section for Z(2b) production as a function of the Z boson p_T, compared with the MADGRAPH 5FS, MADGRAPH 4FS, MADGRAPH5_aMC@NLO, and POWHEG MINLO theoretical predictions (*shaded bands*), normalized to the theoretical cross sections described in the text. For each data point the statistical and the total (sum in quadrature of statistical and systematic) uncertainties are represented by the *double error bar*. The width of the *shaded bands* represents the uncertainty in the theoretical predictions, and, for NLO calculations, theoretical systematic uncertainties are added in the ratio plots with the *inner darker area* representing the statistical component only

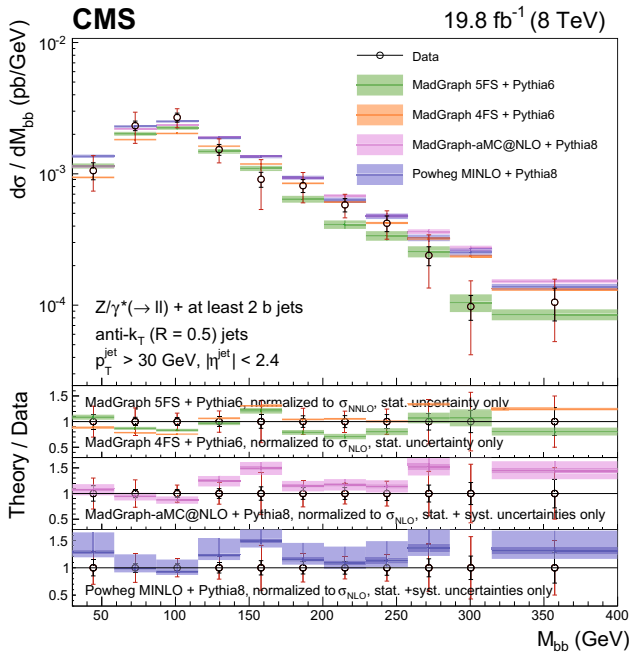

Fig. 12 Differential fiducial cross section for Z(2b) production as a function of the invariant mass of the b jet pair, M_{bb}, compared with the MADGRAPH 5FS, MADGRAPH 4FS, MADGRAPH5_aMC@NLO, and POWHEG MINLO theoretical predictions (*shaded bands*), normalized to the theoretical cross sections described in the text. For each data point the statistical and the total (sum in quadrature of statistical and systematic) uncertainties are represented by the *double error bar*. The width of the *shaded bands* represents the uncertainty in the theoretical predictions, and, for NLO calculations, theoretical systematic uncertainties are added in the ratio plots with the *inner darker area* representing the statistical component only

with MADGRAPH5_aMC@NLO [23] for the 4FS, which has an estimated theoretical uncertainty of 15%, dominated by scale variations. This uncertainty is not shown in the figures.

The event generator MADGRAPH5_aMC@NLO [23] version 2.2.1 is used to provide results at NLO, combining matrix elements for zero, one, and two additional partons through the FXFX algorithm [24]. The NNPDF 3.0 NLO PDF set [26], based on the 5FS, is used. Parton showering and hadronization are performed by PYTHIA version 8.205 [25], using the CUETP8M1 tune [55]. The choice of QCD scales is the same as for the LO MADGRAPH prediction. This is the same event generator that is used in Sect. 3 to study the systematic uncertainty in the secondary vertex mass distribution.

The 5FS is also used to compute the NLO POWHEG prediction for a Z boson associated with two extra partons, including b quarks [56]. Lower parton multiplicities are described in the matrix element as well, but with no guarantee of NLO accuracy. The scale choice is based on the MINLO approach [57]. The NNPDF 3.0 PDF set [26] is used, and the matrix element calculation is matched with the PYTHIA8 parton shower evolution and hadronization, using the CUETP8M1 tune.

For both MADGRAPH5_aMC@NLO and POWHEG, no further rescaling of the native cross section is made. Theoretical systematic uncertainties in the predictions, caused by the choice of the QCD factorization and renormalization scales and by the propagation of the uncertainties in PDFs, are computed. The former are estimated by varying the QCD scales by factors of 2 and 0.5, while the latter are computed according to PDF authors' prescriptions. The uncertainty from varying the QCD scales is generally the dominant contribution. These theoretical uncertainties are displayed in the figures only in the ratio plots, with the statistical uncertainty shown separately, and add up to about 10 and 20% for the two calculations, respectively. For LO calculations, only the statistical uncertainty of theoretical predictions is shown.

8.3 Comparison with data

The measured differential cross sections, unfolded for detector effects, are compatible for the two leptonic channels, and are therefore combined into an uncertainty-weighted average

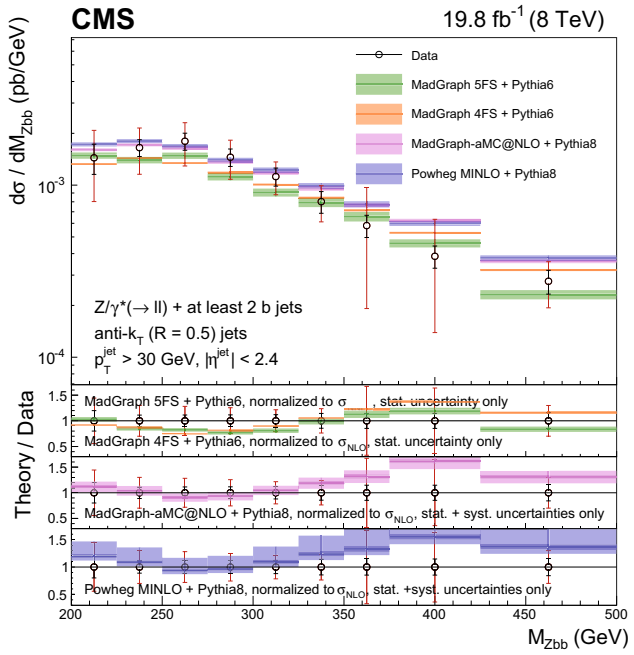

Fig. 13 Differential fiducial cross section for Z(2b) production as a function of the invariant mass of the Zbb system, M_{Zbb}, compared with the MADGRAPH 5FS, MADGRAPH 4FS, MADGRAPH5_aMC@NLO, and POWHEG MINLO theoretical predictions (*shaded bands*), normalized to the theoretical cross sections described in the text. For each data point the statistical and the total (sum in quadrature of statistical and systematic) uncertainties are represented by the *double error bar*. The width of the *shaded bands* represents the uncertainty in the theoretical predictions, and, for NLO calculations, theoretical systematic uncertainties are added in the ratio plots with the *inner darker area* representing the statistical component only

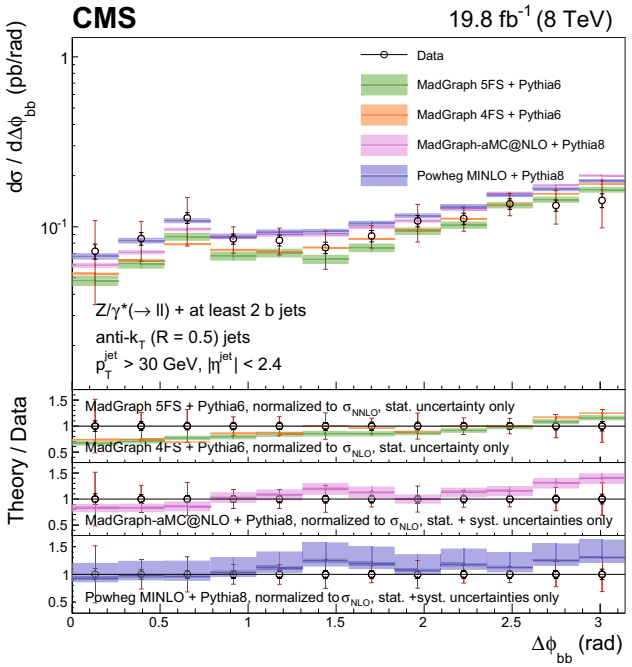

Fig. 14 Differential fiducial cross section for Z(2b) production as a function of $\Delta\phi_{\mathrm{bb}}$, compared with the MADGRAPH 5FS, MADGRAPH 4FS, MADGRAPH5_aMC@NLO, and POWHEG MINLO theoretical predictions (*shaded bands*), normalized to the theoretical cross sections described in the text. For each data point the statistical and the total (sum in quadrature of statistical and systematic) uncertainties are represented by the *double error bar*. The width of the *shaded bands* represents the uncertainty in the theoretical predictions, and, for NLO calculations, theoretical systematic uncertainties are added in the ratio plots with the *inner darker area* representing the statistical component only

for a single lepton flavour. Correlations between systematic uncertainties for the electron and muon channels are taken into account in the combination. In particular, all uncertainties are treated as fully correlated, with the exception of those related to lepton efficiencies, $\mathrm{t\bar{t}}$ background estimates, and the statistical part of the subtraction of the c quark and udsg components from Z+jets, and the statistical part of the unfolding uncertainty, which are treated as fully uncorrelated. All the cross sections are measured in the fiducial phase space defined at the generated particle level for the unfolding procedure, as discussed in Sect. 6. No attempt is made to disentangle b jet production in the hard scattering processes and in MPI.

The integral of the unfolded distributions gives the fiducial cross section, for a single lepton type, for the production of Z(1b) events,

$$\sigma_{\mathrm{fid}}(\mathrm{pp} \to \mathrm{Z} + (\geq 1\mathrm{b})) = 3.55 \pm 0.12\,(\mathrm{stat}) \pm 0.21\,(\mathrm{syst})\ \mathrm{pb},$$

and Z(2b) events,

$$\sigma_{\mathrm{fid}}(\mathrm{pp} \to \mathrm{Z} + (\geq 2\mathrm{b})) = 0.331 \pm 0.011\,(\mathrm{stat}) \pm 0.035\,(\mathrm{syst})\ \mathrm{pb}.$$

These measured values can be compared with the corresponding predictions at NLO of MADGRAPH5_aMC@NLO interfaced with PYTHIA8 (described in Sect. 8.2), $4.23^{+0.27}_{-0.37}$ pb for Z(1b) and $0.356^{+0.030}_{-0.031}$ pb for Z(2b). The prediction overestimates by about 20% the measured value for Z(1b), while a reasonable agreement is found for Z(2b) within uncertainties.

The ratio of the cross sections in the fiducial phase space for the production of at least two and at least one b jet is

$$\frac{\sigma_{\mathrm{fid}}(\mathrm{pp} \to \mathrm{Z} + (\geq 2\mathrm{b}))}{\sigma_{\mathrm{fid}}(\mathrm{pp} \to \mathrm{Z} + (\geq 1\mathrm{b}))} = 0.093 \pm 0.004\,(\mathrm{stat}) \pm 0.007\,(\mathrm{syst}),$$

to be compared with the theoretical prediction $0.084^{+0.002}_{-0.001}$ where the systematic uncertainties are considered as fully correlated.

Results for the differential cross sections for the Z(1b) events are presented in Figs. 4, 5, 6, 7 and 8, together with the ratios to the corresponding observables for the inclusive Z+jets event selection. Where applicable, the last bin also includes overflow values. A discrepancy of about 20% is seen in the overall normalization for the 4FS-based prediction, of the same order of magnitude as its estimated theoretical

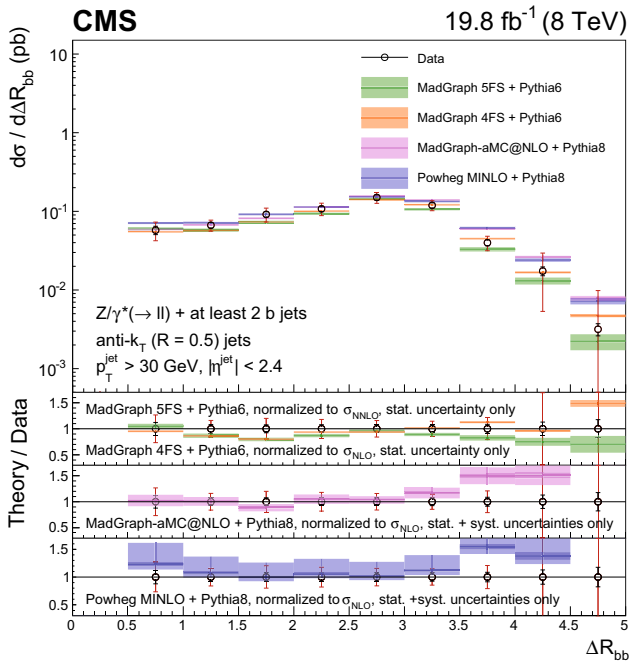

Fig. 15 Differential fiducial cross section for Z(2b) production as a function of ΔR_{bb}, compared with the MADGRAPH 5FS, MADGRAPH 4FS, MADGRAPH5_aMC@NLO, and POWHEG MINLO theoretical predictions (*shaded bands*), normalized to the theoretical cross sections described in the text. For each data point the statistical and the total (sum in quadrature of statistical and systematic) uncertainties are represented by the *double error bar*. The width of the *shaded bands* represents the uncertainty in the theoretical predictions, and, for NLO calculations, theoretical systematic uncertainties are added in the ratio plots with the *inner darker area* representing the statistical component only

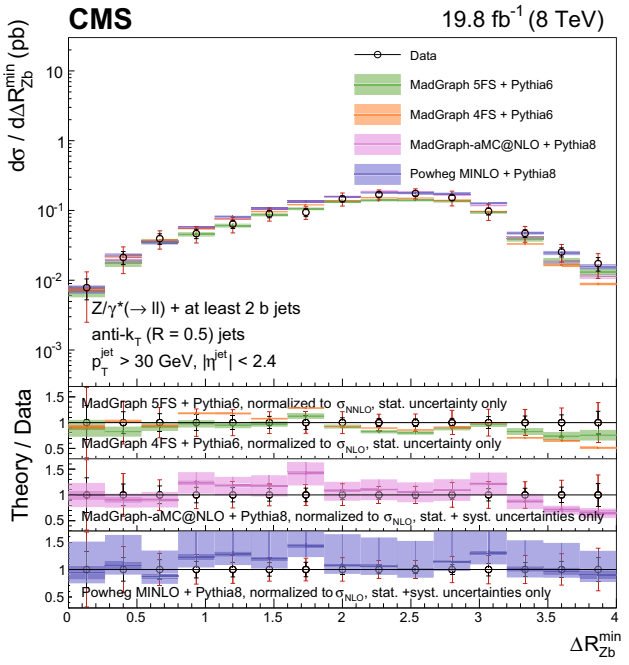

Fig. 16 Differential fiducial cross section for Z(2b) production as a function of $\Delta R_{\mathrm{Zb}}^{\mathrm{min}}$, compared with the MADGRAPH 5FS, MADGRAPH 4FS, MADGRAPH5_aMC@NLO, and POWHEG MINLO theoretical predictions (*shaded bands*), normalized to the theoretical cross sections described in the text. For each data point the statistical and the total (sum in quadrature of statistical and systematic) uncertainties are represented by the *double error bar*. The width of the *shaded bands* represents the uncertainty in the theoretical predictions, and, for NLO calculations, theoretical systematic uncertainties are added in the ratio plots with the *inner darker area* representing the statistical component only

uncertainty. The POWHEG prediction tends to overestimate the cross sections by about 25%.

Apart for the normalization difference, the pQCD calculation with massive b quarks (4FS) seems to reproduce, slightly better, the shape of the observed distributions in the soft momentum regime of b jets. For the leading b jet p_{T} spectrum (Fig. 4), the ratio with data is reasonably flat below 80 GeV, whereas it presents a clear slope in the higher p_{T} range. A similar behaviour is clear in the Z boson p_{T} distribution below 130 GeV (Fig. 6) and in the H_{T} spectrum below 200 GeV (Fig. 7). The POWHEG generator considerably overestimates the soft parts of the p_{T} and H_{T} spectra. The leading b jet $|\eta|$ spectrum shape is well reproduced by the MADGRAPH 4FS configuration (Fig. 5), while MADGRAPH 5FS calculation slightly overestimates the central part of the spectrum. The shape of the distribution of the azimuthal angular separation $\Delta\phi_{\mathrm{Zb}}$ between the Z boson and the leading b jet is reproduced within uncertainties by all the calculations (Fig. 8). The NLO MADGRAPH5_aMC@NLO predictions have similar behaviour to those from LO MADGRAPH 5FS. As far as the NLO POWHEG-based prediction is concerned, it shows a similar behaviour to MADGRAPH5_aMC@NLO, but the discrepancies are larger, reaching about 40% at the peak of the Z boson p_{T} spectrum. In general, the shape predicted by each calculation compares with data, within uncertainties, in a similar way in the high Z boson p_{T} and H_{T} regions, which are potentially sensitive to new physics contributions.

The underestimation of the normalization by MADGRAPH 4FS and the overestimation by POWHEG are also observed in the ratio of Z(1b) and inclusive Z+jets processes (described by the MADGRAPH generator in the 5FS). The pseudorapidity distribution (Fig. 5), with an almost flat shape, clearly shows that the ratio for the 4FS-based prediction is about 4%, compared to the 5% of the 5FS-based calculations, while POWHEG predicts about 6%. The 4FS prediction also fails to reproduce the ratio of the leading jet p_{T} spectra (Fig. 4), which is clearly underestimated below 80 GeV. In contrast, POWHEG overestimates the spectrum in the soft region by about 30%. Similar discrepancies, although less pronounced, are observed for H_{T} and the Z boson p_{T}. The ratio as a function of the azimuthal separation between the Z boson and the b jet (Fig. 8) is also slightly underestimated by the MADGRAPH 4FS prediction when the Z boson is approximately back-to-back with respect to the leading b jet, with a difference in the azimuthal angles close to π.

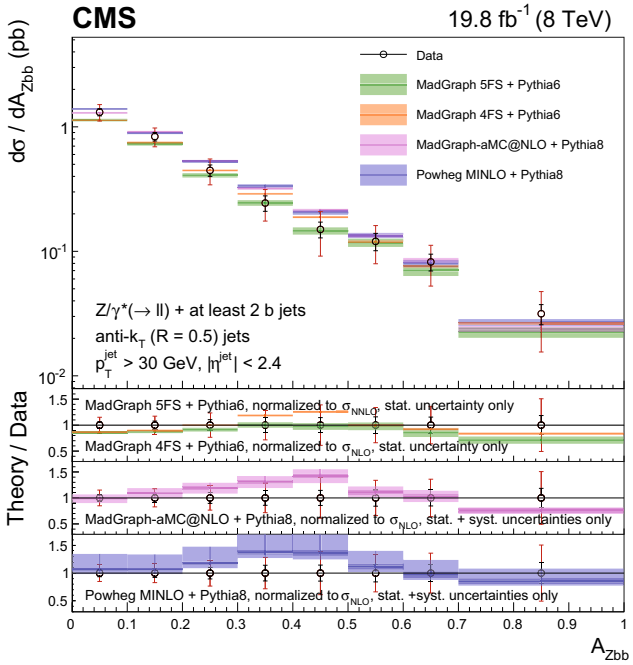

Fig. 17 Differential fiducial cross section for Z(2b) production as a function of A_{Zbb}, compared with the MADGRAPH 5FS, MADGRAPH 4FS, MADGRAPH5_aMC@NLO, and POWHEG MINLO theoretical predictions (*shaded bands*), normalized to the theoretical cross sections described in the text. For each data point the statistical and the total (sum in quadrature of statistical and systematic) uncertainties are represented by the *double error bar*. The width of the *shaded bands* represents the uncertainty in the theoretical predictions, and, for NLO calculations, theoretical systematic uncertainties are added in the ratio plots with the *inner darker area* representing the statistical component only

The results for the differential cross sections measured with the Z(2b) event selection are shown in Figs. 9, 10, 11, 12, 13, 14, 15, 16 and 17. Within uncertainties, no global normalization discrepancy is observed, contrary to the Z(1b) case. The leading and subleading jet spectra are slightly underestimated in the soft region by the LO calculations (the leading b jet p_{T} in the first two bins of Fig. 9 and the subleading b jet p_{T} in the first bin of Fig. 10), while the Z boson p_{T} distribution is well reproduced, within uncertainties (Fig. 11). The 4FS predictions overestimate the data at the high end of these p_{T} distributions. The ratios of all theoretical predictions and the data show a slight positive slope for the azimuthal separation (Fig. 14). All the other distributions are well reproduced. In general, given the experimental uncertainties, the measurements do not strongly discriminate between the theoretical predictions. The ratio of the MADGRAPH5_aMC@NLO and POWHEG predictions based on NLO matrix elements with data shows a similar shape.

9 Summary

The process of associated production of jets, including b jets, and a Z boson decaying into lepton pairs ($\ell = \mathrm{e}, \mu$) are measured in LHC pp collisions at $\sqrt{s} = 8\,\mathrm{TeV}$ with the CMS experiment, using a data set corresponding to an integrated luminosity of $19.8\,\mathrm{fb}^{-1}$. The measured fiducial cross sections are compared to several theoretical predictions. The cross sections are measured as a function of various kinematic observables describing the event topology with a Z boson and at least one b jet: the p_{T} and η of the leading b jet, the Z boson p_{T}, the scalar sum H_{T} of the jet transverse momenta, and the azimuthal angular difference between the directions of the leading b jet and the Z boson. A comparison is made of the unfolded data with leading-order pQCD predictions based on matrix element calculations matched with parton showering, testing models using the MADGRAPH event generator, or with the NLO calculations, merging predictions for zero, one, and two extra jets with MADGRAPH5_aMC@NLO, or for the first two jets with POWHEG in the MINLO approach. In most cases the theoretical predictions agree with the data, although the normalization for MADGRAPH 4FS, which fails to describe simultaneously both the low- and high-p_{T} b jet regions, is underestimated by 20%. The ratios of differential cross sections for the production of a Z boson in association with at least one b jet and the inclusive Z+jets production are measured and compared with theoretical expectations. The 4FS-based prediction fails to describe the shape of the ratio as a function of the leading b jet p_{T}, and discrepancies in the shape are also observed for high values of the Z boson p_{T}.

The production of a Z boson in association with two b jets is also investigated. In this case the kinematic observables are the transverse momenta of the leading and subleading b jets, the p_{T} of the Z boson, the separations of the b jets both in azimuthal angle and in the η–ϕ plane, the minimal distance in the η–ϕ plane between the Z boson and a b jet, the asymmetry between the minimal and the maximal distances between the Z boson and a b jet, and the invariant masses of the bb and the Zbb systems. The measured distributions are generally well reproduced by the predictions.

Acknowledgements We congratulate our colleagues in the CERN accelerator departments for the excellent performance of the LHC and thank the technical and administrative staffs at CERN and at other CMS institutes for their contributions to the success of the CMS effort. In addition, we gratefully acknowledge the computing centres and personnel of the Worldwide LHC Computing Grid for delivering so effectively the computing infrastructure essential to our analyses. Finally, we acknowledge the enduring support for the construction and operation of the LHC and the CMS detector provided by the following funding agencies: the Austrian Federal Ministry of Science, Research and Economy and the Austrian Science Fund; the Belgian Fonds de la Recherche Scientifique, and Fonds voor Wetenschappelijk Onderzoek; the Brazilian Funding Agencies (CNPq, CAPES, FAPERJ, and FAPESP); the Bulgarian Ministry of Education and Science; CERN; the Chinese Academy of Sciences, Ministry of Science and Technology, and National Natural Science Foundation of China; the Colombian Funding Agency (COLCIENCIAS); the Croatian Ministry of Science, Education and Sport, and the Croatian Science Foundation; the Research Promotion Foundation, Cyprus; the Secretariat for Higher Education, Science, Technology and Innovation, Ecuador; the Ministry of Educa-

tion and Research, Estonian Research Council via IUT23-4 and IUT23-6 and European Regional Development Fund, Estonia; the Academy of Finland, Finnish Ministry of Education and Culture, and Helsinki Institute of Physics; the Institut National de Physique Nucléaire et de Physique des Particules / CNRS, and Commissariat à l'Énergie Atomique et aux Énergies Alternatives / CEA, France; the Bundesministerium für Bildung und Forschung, Deutsche Forschungsgemeinschaft, and Helmholtz-Gemeinschaft Deutscher Forschungszentren, Germany; the General Secretariat for Research and Technology, Greece; the National Scientific Research Foundation, and National Innovation Office, Hungary; the Department of Atomic Energy and the Department of Science and Technology, India; the Institute for Studies in Theoretical Physics and Mathematics, Iran; the Science Foundation, Ireland; the Istituto Nazionale di Fisica Nucleare, Italy; the Ministry of Science, ICT and Future Planning, and National Research Foundation (NRF), Republic of Korea; the Lithuanian Academy of Sciences; the Ministry of Education, and University of Malaya (Malaysia); the Mexican Funding Agencies (BUAP, CINVESTAV, CONACYT, LNS, SEP, and UASLP-FAI); the Ministry of Business, Innovation and Employment, New Zealand; the Pakistan Atomic Energy Commission; the Ministry of Science and Higher Education and the National Science Centre, Poland; the Fundação para a Ciência e a Tecnologia, Portugal; JINR, Dubna; the Ministry of Education and Science of the Russian Federation, the Federal Agency of Atomic Energy of the Russian Federation, Russian Academy of Sciences, and the Russian Foundation for Basic Research; the Ministry of Education, Science and Technological Development of Serbia; the Secretaría de Estado de Investigación, Desarrollo e Innovación and Programa Consolider-Ingenio 2010, Spain; the Swiss Funding Agencies (ETH Board, ETH Zurich, PSI, SNF, UniZH, Canton Zurich, and SER); the Ministry of Science and Technology, Taipei; the Thailand Center of Excellence in Physics, the Institute for the Promotion of Teaching Science and Technology of Thailand, Special Task Force for Activating Research and the National Science and Technology Development Agency of Thailand; the Scientific and Technical Research Council of Turkey, and Turkish Atomic Energy Authority; the National Academy of Sciences of Ukraine, and State Fund for Fundamental Researches, Ukraine; the Science and Technology Facilities Council, UK; the US Department of Energy, and the US National Science Foundation. Individuals have received support from the Marie-Curie programme and the European Research Council and EPLANET (European Union); the Leventis Foundation; the A. P. Sloan Foundation; the Alexander von Humboldt Foundation; the Belgian Federal Science Policy Office; the Fonds pour la Formation à la Recherche dans l'Industrie et dans l'Agriculture (FRIA-Belgium); the Agentschap voor Innovatie door Wetenschap en Technologie (IWT-Belgium); the Ministry of Education, Youth and Sports (MEYS) of the Czech Republic; the Council of Science and Industrial Research, India; the HOMING PLUS programme of the Foundation for Polish Science, cofinanced from European Union, Regional Development Fund, the Mobility Plus programme of the Ministry of Science and Higher Education, the National Science Center (Poland), contracts Harmonia 2014/14/M/ST2/00428, Opus 2013/11/B/ST2/04202, 2014/13/B/ST2/02543 and 2014/15/B/ST2/03998, Sonata-bis 2012/07/E/ST2/01406; the Thalis and Aristeia programmes cofinanced by EU-ESF and the Greek NSRF; the National Priorities Research Program by Qatar National Research Fund; the Programa Clarín-COFUND del Principado de Asturias; the Rachadapisek Sompot Fund for Postdoctoral Fellowship, Chulalongkorn University and the Chulalongkorn Academic into Its 2nd Century Project Advancement Project (Thailand); and the Welch Foundation, contract C-1845.

References

1. CMS Collaboration, Search for the standard model Higgs boson produced in association with a W or a Z boson and decaying to bottom quarks. Phys. Rev. D **89**, 012003 (2014). https://doi.org/10.1103/PhysRevD.89.012003. arXiv:1310.3687
2. B. Holdom et al., Four statements about the fourth generation. PMC Phys. A **3**, 4 (2009). https://doi.org/10.1186/1754-0410-3-4. arXiv:0904.4698
3. L.J. Hall, D. Pinner, J.T. Ruderman, A natural SUSY Higgs near 126 GeV. JHEP **04**, 131 (2012). https://doi.org/10.1007/JHEP04(2012)131. arXiv:1112.2703
4. D. Choudhury, T.M.P. Tait, C.E.M. Wagner, Beautiful mirrors and precision electroweak data. Phys. Rev. D **65**, 053002 (2002). https://doi.org/10.1103/PhysRevD.65.053002. arXiv:hep-ph/0109097
5. CDF Collaboration, Measurement of cross sections for b jet production in events with a Z boson in $p\bar{p}$ collisions at $\sqrt{s} = 1.96$ TeV. Phys. Rev. D **79**, 052008 (2009). https://doi.org/10.1103/PhysRevD.79.052008. arXiv:0812.4458
6. D0 Collaboration, A measurement of the ratio of inclusive cross sections $\sigma(p\bar{p} \to Z + \text{bjet})/\sigma(p\bar{p} \to Z + \text{jet})$ at $\sqrt{s} = 1.96$ TeV. Phys. Rev. D **83**, 031105 (2011). https://doi.org/10.1103/PhysRevD.83.031105. arXiv:1010.6203
7. ATLAS Collaboration, Measurement of differential production cross-sections for a Z boson in association with b-jets in 7 TeV proton–proton collisions with the ATLAS detector. JHEP **10**, 141 (2014). https://doi.org/10.1007/JHEP10(2014)141. arXiv:1407.3643
8. CMS Collaboration, Measurement of the production cross sections for a Z boson and one or more b jets in pp collisions at $\sqrt{s} = 7$ TeV. JHEP **06**, 120 (2014). https://doi.org/10.1007/JHEP06(2014)120. arXiv:1402.1521
9. CMS Collaboration, Measurement of the cross section and angular correlations for associated production of a Z boson with b hadrons in pp collisions at $\sqrt{s} = 7$ TeV. JHEP **12**, 039 (2013). https://doi.org/10.1007/JHEP12(2013)039. arXiv:1310.1349
10. D0 Collaboration, Measurement of the ratio of differential cross sections $\sigma(p\bar{p} \to Z + \text{bjet})/\sigma(p\bar{p} \to Z + \text{jet})$ in $p\bar{p}$ collisions at $\sqrt{s} = 1.96$ TeV. Phys. Rev. D **87**, 092010 (2013). https://doi.org/10.1103/PhysRevD.87.092010. arXiv:1301.2233
11. CMS Collaboration, The CMS experiment at the CERN LHC. JINST **3**, S08004 (2008). https://doi.org/10.1088/1748-0221/3/08/S08004
12. CMS Collaboration, Description and performance of track and primary-vertex reconstruction with the CMS tracker. JINST **9**, P10009 (2014). https://doi.org/10.1088/1748-0221/9/10/P10009. arXiv:1405.6569
13. CMS Collaboration, Performance of electron reconstruction and selection with the CMS detector in proton–proton collisions at $\sqrt{s} = 8$ TeV. JINST **10**, P06005 (2015). https://doi.org/10.1088/1748-0221/10/06/P06005. arXiv:1502.02701
14. CMS Collaboration, Performance of CMS muon reconstruction in pp collision events at $\sqrt{s} = 7$ TeV. JINST **7**, P10002 (2012). https://doi.org/10.1088/1748-0221/7/10/P10002. arXiv:1206.4071
15. J. Alwall et al., MadGraph 5: going beyond. JHEP **06**, 128 (2011). https://doi.org/10.1007/JHEP06(2011)128. arXiv:1106.0522
16. J. Pumplin et al., New generation of parton distributions with uncertainties from global QCD analysis. JHEP **07**, 012 (2002). https://doi.org/10.1088/1126-6708/2002/07/012. arXiv:hep-ph/0201195

17. T. Sjöstrand, S. Mrenna, P.Z. Skands, PYTHIA 6.4 physics and manual. JHEP **05**, 026 (2006). https://doi.org/10.1088/1126-6708/2006/05/026. arXiv:hep-ph/0603175
18. CMS Collaboration, Study of the underlying event at forward rapidity in pp collisions at $\sqrt{s} = 0.9, 2.76$, and 7 TeV. JHEP **04**, 072 (2013). https://doi.org/10.1007/JHEP04(2013)072. arXiv:1302.2394
19. J. Alwall et al., Comparative study of various algorithms for the merging of parton showers and matrix elements in hadronic collisions. Eur. Phys. J. C **53**, 473 (2008). https://doi.org/10.1140/epjc/s10052-007-0490-5. arXiv:0706.2569
20. R. Gavin, Y. Li, F. Petriello, S. Quackenbush, FEWZ 2.0: a code for hadronic Z production at next-to-next-to-leading order. Comput. Phys. Commun. **182**, 2388 (2011). https://doi.org/10.1016/j.cpc.2011.06.008. arXiv:1011.3540
21. Y. Li, F. Petriello, Combining QCD and electroweak corrections to dilepton production in FEWZ. Phys. Rev. D **86**, 094034 (2012). https://doi.org/10.1103/PhysRevD.86.094034. arXiv:1208.5967
22. M. Czakon, P. Fiedler, A. Mitov, Total top-quark pair-production cross section at hadron colliders through $\mathcal{O}(\alpha_S^4)$. Phys. Rev. Lett. **110**, 252004 (2013). https://doi.org/10.1103/PhysRevLett.110.252004. arXiv:1303.6254
23. J. Alwall et al., The automated computation of tree-level and next-to-leading order differential cross sections, and their matching to parton shower simulations. JHEP **07**, 079 (2014). https://doi.org/10.1007/JHEP07(2014)079. arXiv:1405.0301
24. R. Frederix, S. Frixione, Merging meets matching in MC@NLO. JHEP **12**, 061 (2012). https://doi.org/10.1007/JHEP12(2012)061. arXiv:1209.6215
25. T. Sjöstrand, S. Mrenna, P.Z. Skands, A brief introduction to PYTHIA 8.1. Comput. Phys. Commun. **178**, 852 (2008). https://doi.org/10.1016/j.cpc.2008.01.036. arXiv:0710.3820
26. NNPDF Collaboration, Parton distributions for the LHC Run II. JHEP **04**, 040 (2015). https://doi.org/10.1007/JHEP04(2015)040. arXiv:1410.8849
27. J.M. Campbell, R.K. Ellis, C. Williams, Vector boson pair production at the LHC. JHEP **07**, 018 (2011). https://doi.org/10.1007/JHEP07(2011)018. arXiv:1105.0020
28. S. Frixione, P. Nason, C. Oleari, Matching NLO QCD computations with parton shower simulations: the POWHEG method. JHEP **11**, 070 (2007). https://doi.org/10.1088/1126-6708/2007/11/070. arXiv:0709.2092
29. P. Nason, A new method for combining NLO QCD with shower Monte Carlo algorithms. JHEP **11**, 040 (2004). https://doi.org/10.1088/1126-6708/2004/11/040. arXiv:hep-ph/0409146
30. S. Alioli, P. Nason, C. Oleari, E. Re, A general framework for implementing NLO calculations in shower Monte Carlo programs: the POWHEG BOX. JHEP **06**, 043 (2010). https://doi.org/10.1007/JHEP06(2010)043. arXiv:1002.2581
31. S. Alioli, P. Nason, C. Oleari, E. Re, NLO single-top production matched with shower in POWHEG: s- and t-channel contributions. JHEP **09**, 111 (2009). https://doi.org/10.1088/1126-6708/2009/09/111. arXiv:0907.4076 [Erratum: 10.1007/JHEP02(2010)011]
32. E. Re, Single-top Wt-channel production matched with parton showers using the POWHEG method. Eur. Phys. J. C **71**, 1547 (2011). https://doi.org/10.1140/epjc/s10052-011-1547-z. arXiv:1009.2450
33. GEANT4 Collaboration, GEANT4—a simulation toolkit. Nucl. Instrum. Methods A **506**, 250 (2003). https://doi.org/10.1016/S0168-9002(03)01368-8
34. CMS Collaboration, Particle-flow event reconstruction in CMS and performance for jets, taus, and E_T^{miss}. CMS Physics Analysis Summary CMS-PAS-PFT-09-001, CERN (2006). https://cds.cern.ch/record/1194487
35. CMS Collaboration, Commissioning of the particle-flow event reconstruction with the first LHC collisions recorded in the CMS detector. CMS Physics Analysis Summary CMS-PAS-PFT-10-001, CERN (2010). https://cds.cern.ch/record/1247373
36. M. Cacciari, G.P. Salam, Pileup subtraction using jet areas. Phys. Lett. B **659**, 119 (2008). https://doi.org/10.1016/j.physletb.2007.09.077. arXiv:0707.1378
37. CMS Collaboration, Measurements of inclusive W and Z cross sections in pp collisions at $\sqrt{s} = 7$ TeV. JHEP **01**, 080 (2011). https://doi.org/10.1007/JHEP01(2011)080. arXiv:1012.2466
38. M. Cacciari, G.P. Salam, G. Soyez, The anti-k_t jet clustering algorithm. JHEP **04**, 063 (2008). https://doi.org/10.1088/1126-6708/2008/04/063. arXiv:0802.1189
39. M. Cacciari, G.P. Salam, G. Soyez, FastJet user manual. Eur. Phys. J. C **72**, 1896 (2012). https://doi.org/10.1140/epjc/s10052-012-1896-2. arXiv:1111.6097
40. CMS Collaboration, Determination of jet energy calibration and transverse momentum resolution in CMS. JINST **6**, P11002 (2011). https://doi.org/10.1088/1748-0221/6/11/P11002. arXiv:1107.4277
41. CMS Collaboration, Jet energy scale and resolution in the CMS experiment in pp collisions at 8 TeV. JINST **12**, P02014 (2017). https://doi.org/10.1088/1748-0221/12/02/P02014. arXiv:1607.03663
42. CMS Collaboration, Identification of b-quark jets with the CMS experiment. JINST **8**, P04013 (2013). https://doi.org/10.1088/1748-0221/8/04/P04013. arXiv:1211.4462
43. CMS Collaboration, Missing transverse energy performance of the CMS detector. JINST **6**, P09001 (2011). https://doi.org/10.1088/1748-0221/6/09/P09001
44. CMS Collaboration, Performance of the CMS missing transverse momentum reconstruction in pp data at $\sqrt{s} = 8$ TeV. JINST **10**, P02006 (2015). https://doi.org/10.1088/1748-0221/10/02/P02006. arXiv:1411.0511
45. CMS Collaboration, Event shapes and azimuthal correlations in Z+jets events in pp collisions at $\sqrt{s} = 7$ TeV. Phys. Lett. B **722**, 238 (2013). https://doi.org/10.1016/j.physletb.2013.04.025. arXiv:1301.1646
46. A. Höcker, V. Kartvelishvili, SVD approach to data unfolding. Nucl. Instrum. Methods A **372**, 469 (1996). https://doi.org/10.1016/0168-9002(95)01478-0. arXiv:hep-ph/9509307
47. T. Adye, Unfolding algorithms and tests using RooUnfold, in *PHYSTAT 2011 Workshop on Statistical Issues Related to Discovery Claims in Search Experiments and Unfolding*, ed. by H. Prosper, L. Lyons (Geneva, 2011), p. 313. https://doi.org/10.5170/CERN-2011-006.313. arXiv:1105.1160
48. G. D'Agostini, A multidimensional unfolding method based on Bayes theorem. Nucl. Instrum. Methods A **362**, 487 (1995). https://doi.org/10.1016/0168-9002(95)00274-X
49. CMS Collaboration, CMS luminosity based on pixel cluster counting—summer 2013 update. CMS Physics Analysis Summary CMS-PAS-LUM-13-001, CERN (2013). https://cds.cern.ch/record/1598864
50. F. Febres Cordero, L. Reina, D. Wackeroth, W and Z boson production with a massive bottom-quark pair at the Large Hadron Collider. Phys. Rev. D **80**, 034015 (2009). https://doi.org/10.1103/PhysRevD.80.034015. arXiv:0906.1923
51. J.M. Campbell, R.K. Ellis, F. Maltoni, S. Willenbrock, Associated production of a Z boson and a single heavy quark jet. Phys. Rev. D **69**, 074021 (2004). https://doi.org/10.1103/PhysRevD.69.074021. arXiv:hep-ph/0312024
52. F. Maltoni, G. Ridolfi, M. Ubiali, b-initiated processes at the LHC: a reappraisal. JHEP **07**, 022 (2012). https://doi.org/10.1007/JHEP07(2012)022. arXiv:1203.6393 [Erratum: JHEP **04**, 095 (2013). doi:10.1007/JHEP04(2013)095]

53. J. Alwall, S. de Visscher, F. Maltoni, QCD radiation in the production of heavy colored particles at the LHC. JHEP **02**, 017 (2009). https://doi.org/10.1088/1126-6708/2009/02/017. arXiv:0810.5350
54. A.D. Martin, W.J. Stirling, R.S. Thorne, G. Watt, Parton distributions for the LHC. Eur. Phys. J. C **63**, 189 (2009). https://doi.org/10.1140/epjc/s10052-009-1072-5. arXiv:0901.0002
55. CMS Collaboration, Event generator tunes obtained from underlying event and multiparton scattering measurements. Eur. Phys. J. C **76**, 155 (2016). https://doi.org/10.1140/epjc/s10052-016-3988-x. arXiv:1512.00815
56. J.M. Campbell, R.K. Ellis, P. Nason, G. Zanderighi, W and Z bosons in association with two jets using the POWHEG method. JHEP **08**, 005 (2013). https://doi.org/10.1007/JHEP08(2013)005. arXiv:1303.5447
57. K. Hamilton, P. Nason, G. Zanderighi, MINLO: multi-scale improved NLO. JHEP **10**, 155 (2012). https://doi.org/10.1007/JHEP10(2012)155. arXiv:1206.3572

CMS Collaboration

Yerevan Physics Institute, Yerevan, Armenia
V. Khachatryan, A. M. Sirunyan, A. Tumasyan

Institut für Hochenergiephysik, Vienna, Austria
W. Adam, E. Asilar, T. Bergauer, J. Brandstetter, E. Brondolin, M. Dragicevic, J. Erö, M. Flechl, M. Friedl, R. Frühwirth[1], V. M. Ghete, C. Hartl, N. Hörmann, J. Hrubec, M. Jeitler[1], A. König, M. Krammer[1], I. Krätschmer, D. Liko, T. Matsushita, I. Mikulec, D. Rabady, N. Rad, B. Rahbaran, H. Rohringer, J. Schieck[1], J. Strauss, W. Treberer-Treberspurg, W. Waltenberger, C.-E. Wulz[1]

National Centre for Particle and High Energy Physics, Minsk, Belarus
V. Mossolov, N. Shumeiko, J. Suarez Gonzalez

Universiteit Antwerpen, Antwerp, Belgium
S. Alderweireldt, T. Cornelis, E. A. De Wolf, X. Janssen, A. Knutsson, J. Lauwers, S. Luyckx, M. Van De Klundert, H. Van Haevermaet, P. Van Mechelen, N. Van Remortel, A. Van Spilbeeck

Vrije Universiteit Brussel, Brussels, Belgium
S. Abu Zeid, F. Blekman, J. D'Hondt, N. Daci, I. De Bruyn, K. Deroover, N. Heracleous, J. Keaveney, S. Lowette, S. Moortgat, L. Moreels, A. Olbrechts, Q. Python, D. Strom, S. Tavernier, W. Van Doninck, P. Van Mulders, I. Van Parijs

Université Libre de Bruxelles, Brussels, Belgium
H. Brun, C. Caillol, B. Clerbaux, G. De Lentdecker, G. Fasanella, L. Favart, R. Goldouzian, A. Grebenyuk, G. Karapostoli, T. Lenzi, A. Léonard, T. Maerschalk, A. Marinov, A. Randle-conde, T. Seva, C. Vander Velde, P. Vanlaer, R. Yonamine, F. Zenoni, F. Zhang[2]

Ghent University, Ghent, Belgium
L. Benucci, A. Cimmino, S. Crucy, D. Dobur, A. Fagot, G. Garcia, M. Gul, J. Mccartin, A. A. Ocampo Rios, D. Poyraz, D. Ryckbosch, S. Salva, R. Schöfbeck, M. Sigamani, M. Tytgat, W. Van Driessche, E. Yazgan, N. Zaganidis

Université Catholique de Louvain, Louvain-la-Neuve, Belgium
C. Beluffi[3], O. Bondu, S. Brochet, G. Bruno, A. Caudron, L. Ceard, S. De Visscher, C. Delaere, M. Delcourt, L. Forthomme, B. Francois, A. Giammanco, A. Jafari, P. Jez, M. Komm, V. Lemaitre, A. Magitteri, A. Mertens, M. Musich, C. Nuttens, K. Piotrzkowski, L. Quertenmont, M. Selvaggi, M. Vidal Marono, S. Wertz

Université de Mons, Mons, Belgium
N. Beliy, G. H. Hammad

Centro Brasileiro de Pesquisas Fisicas, Rio de Janeiro, Brazil
W. L. Aldá Júnior, F. L. Alves, G. A. Alves, L. Brito, M. Correa Martins Junior, M. Hamer, C. Hensel, A. Moraes, M. E. Pol, P. Rebello Teles

Universidade do Estado do Rio de Janeiro, Rio de Janeiro, Brazil
E. Belchior Batista Das Chagas, W. Carvalho, J. Chinellato[4], A. Custódio, E. M. Da Costa, D. De Jesus Damiao, C. De Oliveira Martins, S. Fonseca De Souza, L. M. Huertas Guativa, H. Malbouisson, D. Matos Figueiredo, C. Mora Herrera, L. Mundim, H. Nogima, W. L. Prado Da Silva, A. Santoro, A. Sznajder, E. J. Tonelli Manganote[4], A. Vilela Pereira

Universidade Estadual Paulista[a], Universidade Federal do ABC[b], São Paulo, Brazil
S. Ahuja[a], C. A. Bernardes[b], A. De Souza Santos[b], S. Dogra[a], T. R. Fernandez Perez Tomei[a], E. M. Gregores[b], P. G. Mercadante[b], C. S. Moon[a,5], S. F. Novaes[a], Sandra S. Padula[a], D. Romero Abad[b], J. C. Ruiz Vargas

Institute for Nuclear Research and Nuclear Energy, Sofia, Bulgaria
A. Aleksandrov, R. Hadjiiska, P. Iaydjiev, M. Rodozov, S. Stoykova, G. Sultanov, M. Vutova

University of Sofia, Sofia, Bulgaria
A. Dimitrov, I. Glushkov, L. Litov, B. Pavlov, P. Petkov

Beihang University, Beijing, China
W. Fang[6]

Institute of High Energy Physics, Beijing, China
M. Ahmad, J. G. Bian, G. M. Chen, H. S. Chen, M. Chen, T. Cheng, R. Du, C. H. Jiang, D. Leggat, R. Plestina[7], F. Romeo, S. M. Shaheen, A. Spiezia, J. Tao, C. Wang, Z. Wang, H. Zhang

State Key Laboratory of Nuclear Physics and Technology, Peking University, Beijing, China
C. Asawatangtrakuldee, Y. Ban, Q. Li, S. Liu, Y. Mao, S. J. Qian, D. Wang, Z. Xu

Universidad de Los Andes, Bogotá, Colombia
C. Avila, A. Cabrera, L. F. Chaparro Sierra, C. Florez, J. P. Gomez, B. Gomez Moreno, J. C. Sanabria

Faculty of Electrical Engineering, Mechanical Engineering and Naval Architecture, University of Split, Split, Croatia
N. Godinovic, D. Lelas, I. Puljak, P. M. Ribeiro Cipriano

Faculty of Science, University of Split, Split, Croatia
Z. Antunovic, M. Kovac

Institute Rudjer Boskovic, Zagreb, Croatia
V. Brigljevic, D. Ferencek, K. Kadija, J. Luetic, S. Micanovic, L. Sudic

University of Cyprus, Nicosia, Cyprus
A. Attikis, G. Mavromanolakis, J. Mousa, C. Nicolaou, F. Ptochos, P. A. Razis, H. Rykaczewski

Charles University, Prague, Czech Republic
M. Finger[8], M. Finger Jr.[8]

Universidad San Francisco de Quito, Quito, Ecuador
E. Carrera Jarrin

Egyptian Network of High Energy Physics, Academy of Scientific Research and Technology of the Arab Republic of Egypt, Cairo, Egypt
A. A. Abdelalim[9,10], E. El-khateeb[11], T. Elkafrawy[11], M. A. Mahmoud[12,13]

National Institute of Chemical Physics and Biophysics, Tallinn, Estonia
B. Calpas, M. Kadastik, M. Murumaa, L. Perrini, M. Raidal, A. Tiko, C. Veelken

Department of Physics, University of Helsinki, Helsinki, Finland
P. Eerola, J. Pekkanen, M. Voutilainen

Helsinki Institute of Physics, Helsinki, Finland
J. Härkönen, V. Karimäki, R. Kinnunen, T. Lampén, K. Lassila-Perini, S. Lehti, T. Lindén, P. Luukka, T. Peltola, J. Tuominiemi, E. Tuovinen, L. Wendland

Lappeenranta University of Technology, Lappeenranta, Finland
J. Talvitie, T. Tuuva

IRFU, CEA, Université Paris-Saclay, Gif-sur-Yvette, France
M. Besancon, F. Couderc, M. Dejardin, D. Denegri, B. Fabbro, J. L. Faure, C. Favaro, F. Ferri, S. Ganjour, A. Givernaud, P. Gras, G. Hamel de Monchenault, P. Jarry, E. Locci, M. Machet, J. Malcles, J. Rander, A. Rosowsky, M. Titov, A. Zghiche

Laboratoire Leprince-Ringuet, Ecole Polytechnique, IN2P3-CNRS, Palaiseau, France
A. Abdulsalam, I. Antropov, S. Baffioni, F. Beaudette, P. Busson, L. Cadamuro, E. Chapon, C. Charlot, O. Davignon, L. Dobrzynski, R. Granier de Cassagnac, M. Jo, S. Lisniak, P. Miné, I. N. Naranjo, M. Nguyen, C. Ochando, G. Ortona, P. Paganini, P. Pigard, S. Regnard, R. Salerno, Y. Sirois, T. Strebler, Y. Yilmaz, A. Zabi

Institut Pluridisciplinaire Hubert Curien, Université de Strasbourg, Université de Haute Alsace Mulhouse, CNRS/IN2P3, Strasbourg, France
J.-L. Agram[14], J. Andrea, A. Aubin, D. Bloch, J.-M. Brom, M. Buttignol, E. C. Chabert, N. Chanon, C. Collard, E. Conte[14], X. Coubez, J.-C. Fontaine[14], D. Gelé, U. Goerlach, C. Goetzmann, A.-C. Le Bihan, J. A. Merlin[15], K. Skovpen, P. Van Hove

Centre de Calcul de l'Institut National de Physique Nucleaire et de Physique des Particules, CNRS/IN2P3, Villeurbanne, France
S. Gadrat

Institut de Physique Nucléaire de Lyon, Université de Lyon, Université Claude Bernard Lyon 1, CNRS-IN2P3, Villeurbanne, France
S. Beauceron, C. Bernet, G. Boudoul, E. Bouvier, C. A. Carrillo Montoya, R. Chierici, D. Contardo, B. Courbon, P. Depasse, H. El Mamouni, J. Fan, J. Fay, S. Gascon, M. Gouzevitch, B. Ille, F. Lagarde, I. B. Laktineh, M. Lethuillier, L. Mirabito, A. L. Pequegnot, S. Perries, A. Popov[16], J. D. Ruiz Alvarez, D. Sabes, V. Sordini, M. Vander Donckt, P. Verdier, S. Viret

Georgian Technical University, Tbilisi, Georgia
T. Toriashvili[17]

Tbilisi State University, Tbilisi, Georgia
I. Bagaturia[18]

I. Physikalisches Institut, RWTH Aachen University, Aachen, Germany
C. Autermann, S. Beranek, L. Feld, A. Heister, M. K. Kiesel, K. Klein, M. Lipinski, A. Ostapchuk, M. Preuten, F. Raupach, S. Schael, C. Schomakers, J. F. Schulte, J. Schulz, T. Verlage, H. Weber, V. Zhukov[16]

III. Physikalisches Institut A, RWTH Aachen University, Aachen, Germany
M. Ata, M. Brodski, E. Dietz-Laursonn, D. Duchardt, M. Endres, M. Erdmann, S. Erdweg, T. Esch, R. Fischer, A. Güth, T. Hebbeker, C. Heidemann, K. Hoepfner, S. Knutzen, M. Merschmeyer, A. Meyer, P. Millet, S. Mukherjee, M. Olschewski, K. Padeken, P. Papacz, T. Pook, M. Radziej, H. Reithler, M. Rieger, F. Scheuch, L. Sonnenschein, D. Teyssier, S. Thüer

III. Physikalisches Institut B, RWTH Aachen University, Aachen, Germany
V. Cherepanov, Y. Erdogan, G. Flügge, H. Geenen, M. Geisler, F. Hoehle, B. Kargoll, T. Kress, A. Künsken, J. Lingemann, A. Nehrkorn, A. Nowack, I. M. Nugent, C. Pistone, O. Pooth, A. Stahl[15]

Deutsches Elektronen-Synchrotron, Hamburg, Germany
M. Aldaya Martin, I. Asin, K. Beernaert, O. Behnke, U. Behrens, K. Borras[19], A. Campbell, P. Connor, C. Contreras-Campana, F. Costanza, C. Diez Pardos, G. Dolinska, S. Dooling, G. Eckerlin, D. Eckstein, T. Eichhorn, E. Gallo[20], J. Garay Garcia, A. Geiser, A. Gizhko, J. M. Grados Luyando, P. Gunnellini, A. Harb, J. Hauk, M. Hempel[21], H. Jung, A. Kalogeropoulos, O. Karacheban[21], M. Kasemann, J. Kieseler, C. Kleinwort, I. Korol, W. Lange, A. Lelek, J. Leonard, K. Lipka, A. Lobanov, W. Lohmann[21], R. Mankel, I.-A. Melzer-Pellmann, A. B. Meyer, G. Mittag, J. Mnich, A. Mussgiller, E. Ntomari, D. Pitzl, R. Placakyte, A. Raspereza, B. Roland, M. Ö. Sahin, P. Saxena, T. Schoerner-Sadenius, C. Seitz, S. Spannagel, N. Stefaniuk, K. D. Trippkewitz, G. P. Van Onsem, R. Walsh, C. Wissing

University of Hamburg, Hamburg, Germany
V. Blobel, M. Centis Vignali, A. R. Draeger, T. Dreyer, J. Erfle, E. Garutti, K. Goebel, D. Gonzalez, M. Görner, J. Haller, M. Hoffmann, R. S. Höing, A. Junkes, R. Klanner, R. Kogler, N. Kovalchuk, T. Lapsien, T. Lenz, I. Marchesini, D. Marconi, M. Meyer, M. Niedziela, D. Nowatschin, J. Ott, F. Pantaleo[15], T. Peiffer, A. Perieanu, N. Pietsch, J. Poehlsen, C. Sander, C. Scharf, P. Schleper, E. Schlieckau, A. Schmidt, S. Schumann, J. Schwandt, H. Stadie, G. Steinbrück, F. M. Stober, H. Tholen, D. Troendle, E. Usai, L. Vanelderen, A. Vanhoefer, B. Vormwald

Institut für Experimentelle Kernphysik, Karlsruhe, Germany
C. Barth, C. Baus, J. Berger, C. Böser, E. Butz, T. Chwalek, F. Colombo, W. De Boer, A. Descroix, A. Dierlamm, S. Fink, F. Frensch, R. Friese, M. Giffels, A. Gilbert, D. Haitz, F. Hartmann[15], S. M. Heindl, U. Husemann, I. Katkov[16], A. Kornmayer[15], P. Lobelle Pardo, B. Maier, H. Mildner, M. U. Mozer, T. Müller, Th. Müller, M. Plagge, G. Quast, K. Rabbertz, S. Röcker, F. Roscher, M. Schröder, G. Sieber, H. J. Simonis, R. Ulrich, J. Wagner-Kuhr, S. Wayand, M. Weber, T. Weiler, S. Williamson, C. Wöhrmann, R. Wolf

Institute of Nuclear and Particle Physics (INPP), NCSR Demokritos, Aghia Paraskevi, Greece
G. Anagnostou, G. Daskalakis, T. Geralis, V. A. Giakoumopoulou, A. Kyriakis, D. Loukas, A. Psallidas, I. Topsis-Giotis

National and Kapodistrian University of Athens, Athens, Greece
A. Agapitos, S. Kesisoglou, A. Panagiotou, N. Saoulidou, E. Tziaferi

University of Ioánnina, Ioannina, Greece
I. Evangelou, G. Flouris, C. Foudas, P. Kokkas, N. Loukas, N. Manthos, I. Papadopoulos, E. Paradas, J. Strologas

MTA-ELTE Lendület CMS Particle and Nuclear Physics Group, Eötvös Loránd University, Budapest, Hungary
N. Filipovic

Wigner Research Centre for Physics, Budapest, Hungary
G. Bencze, C. Hajdu, P. Hidas, D. Horvath[22], F. Sikler, V. Veszpremi, G. Vesztergombi[23], A. J. Zsigmond

Institute of Nuclear Research ATOMKI, Debrecen, Hungary
N. Beni, S. Czellar, J. Karancsi[24], J. Molnar, Z. Szillasi

Institute of Physics, University of Debrecen, Debrecen, Hungary
M. Bartók[23], A. Makovec, P. Raics, Z. L. Trocsanyi, B. Ujvari

National Institute of Science Education and Research, Bhubaneswar, India
S. Choudhury[25], P. Mal, K. Mandal, A. Nayak, D. K. Sahoo, N. Sahoo, S. K. Swain

Panjab University, Chandigarh, India
S. Bansal, S. B. Beri, V. Bhatnagar, R. Chawla, R. Gupta, U. Bhawandeep, A. K. Kalsi, A. Kaur, M. Kaur, R. Kumar, A. Mehta, M. Mittal, J. B. Singh, G. Walia

University of Delhi, Delhi, India
Ashok Kumar, A. Bhardwaj, B. C. Choudhary, R. B. Garg, S. Keshri, A. Kumar, S. Malhotra, M. Naimuddin, N. Nishu, K. Ranjan, R. Sharma, V. Sharma

Saha Institute of Nuclear Physics, Kolkata, India
R. Bhattacharya, S. Bhattacharya, K. Chatterjee, S. Dey, S. Dutta, S. Ghosh, N. Majumdar, A. Modak, K. Mondal, S. Mukhopadhyay, S. Nandan, A. Purohit, A. Roy, D. Roy, S. Roy Chowdhury, S. Sarkar, M. Sharan

Bhabha Atomic Research Centre, Mumbai, India
R. Chudasama, D. Dutta, V. Jha, V. Kumar, A. K. Mohanty[15], L. M. Pant, P. Shukla, A. Topkar

Indian Institute of Science Education and Research (IISER), Pune, India
S. Chauhan, S. Dube, A. Kapoor, K. Kothekar, A. Rane, S. Sharma

Institute for Research in Fundamental Sciences (IPM), Tehran, Iran
H. Bakhshiansohi, H. Behnamian, S. M. Etesami[26], A. Fahim[27], M. Khakzad, M. Mohammadi Najafabadi, M. Naseri, S. Paktinat Mehdiabadi, F. Rezaei Hosseinabadi, B. Safarzadeh[28], M. Zeinali

University College Dublin, Dublin, Ireland
M. Felcini, M. Grunewald

INFN Sezione di Bari[a], Università di Bari[b], Politecnico di Bari[c], Bari, Italy
M. Abbrescia[a,b], C. Calabria[a,b], C. Caputo[a,b], A. Colaleo[a], D. Creanza[a,c], L. Cristella[a,b], N. De Filippis[a,c], M. De Palma[a,b], L. Fiore[a], G. Iaselli[a,c], G. Maggi[a,c], M. Maggi[a], G. Miniello[a,b], S. My[a,b], S. Nuzzo[a,b], A. Pompili[a,b], G. Pugliese[a,c], R. Radogna[a,b], A. Ranieri[a], G. Selvaggi[a,b], L. Silvestris[a,15], R. Venditti[a,b]

INFN Sezione di Bologna[a], Università di Bologna[b], Bologna, Italy
G. Abbiendi[a], C. Battilana, D. Bonacorsi[a,b], S. Braibant-Giacomelli[a,b], L. Brigliadori[a,b], R. Campanini[a,b], P. Capiluppi[a,b], A. Castro[a,b], F. R. Cavallo[a], S. S. Chhibra[a,b], G. Codispoti[a,b], M. Cuffiani[a,b], G. M. Dallavalle[a], F. Fabbri[a], A. Fanfani[a,b], D. Fasanella[a,b], P. Giacomelli[a], C. Grandi[a], L. Guiducci[a,b], S. Marcellini[a], G. Masetti[a], A. Montanari[a], F. L. Navarria[a,b], A. Perrotta[a], A. M. Rossi[a,b], T. Rovelli[a,b], G. P. Siroli[a,b], N. Tosi[a,b,15]

INFN Sezione di Catania[a], Università di Catania[b], Catania, Italy
G. Cappello[b], M. Chiorboli[a,b], S. Costa[a,b], A. Di Mattia[a], F. Giordano[a,b], R. Potenza[a,b], A. Tricomi[a,b], C. Tuve[a,b]

INFN Sezione di Firenze[a], Università di Firenze[b], Florence, Italy
G. Barbagli[a], V. Ciulli[a,b], C. Civinini[a], R. D'Alessandro[a,b], E. Focardi[a,b], V. Gori[a,b], P. Lenzi[a,b], M. Meschini[a], S. Paoletti[a], G. Sguazzoni[a], L. Viliani[a,b,15]

INFN Laboratori Nazionali di Frascati, Frascati, Italy
L. Benussi, S. Bianco, F. Fabbri, D. Piccolo, F. Primavera[15]

INFN Sezione di Genova[a], Università di Genova[b], Genoa, Italy
V. Calvelli[a,b], F. Ferro[a], M. Lo Vetere[a,b], M. R. Monge[a,b], E. Robutti[a], S. Tosi[a,b]

INFN Sezione di Milano-Bicocca[a], Università di Milano-Bicocca[b], Milan, Italy
L. Brianza, M. E. Dinardo[a,b], S. Fiorendi[a,b], S. Gennai[a], A. Ghezzi[a,b], P. Govoni[a,b], S. Malvezzi[a], R. A. Manzoni[a,b,15], B. Marzocchi[a,b], D. Menasce[a], L. Moroni[a], M. Paganoni[a,b], D. Pedrini[a], S. Pigazzini, S. Ragazzi[a,b], N. Redaelli[a], T. Tabarelli de Fatis[a,b]

INFN Sezione di Napoli[a], Università di Napoli 'Federico II' [b], Napoli, Italy, Università della Basilicata [c], Potenza, Italy, Università G. Marconi[d], Rome, Italy
S. Buontempo[a], N. Cavallo[a,c], S. Di Guida[a,d,15], M. Esposito[a,b], F. Fabozzi[a,c], A. O. M. Iorio[a,b], G. Lanza[a], L. Lista[a], S. Meola[a,d,15], M. Merola[a], P. Paolucci[a,15], C. Sciacca[a,b], F. Thyssen

INFN Sezione di Padova[a], Università di Padova[b], Padua, Italy, Università di Trento[c], Trento, Italy
P. Azzi[a,15], N. Bacchetta[a], L. Benato[a,b], D. Bisello[a,b], A. Boletti[a,b], R. Carlin[a,b], P. Checchia[a], M. Dall'Osso[a,b], P. De Castro Manzano[a], T. Dorigo[a], U. Dosselli[a], F. Gasparini[a,b], U. Gasparini[a,b], A. Gozzelino[a], K. Kanishchev[a,c], S. Lacaprara[a], M. Margoni[a,b], A. T. Meneguzzo[a,b], J. Pazzini[a,b,15], N. Pozzobon[a,b], P. Ronchese[a,b], F. Simonetto[a,b], E. Torassa[a], M. Tosi[a,b], S. Vanini[a,b], S. Ventura[a], M. Zanetti, P. Zotto[a,b], A. Zucchetta[a,b], G. Zumerle[a,b]

INFN Sezione di Pavia[a], Università di Pavia[b], Pavia, Italy
A. Braghieri[a], A. Magnani[a,b], P. Montagna[a,b], S. P. Ratti[a,b], V. Re[a], C. Riccardi[a,b], P. Salvini[a], I. Vai[a,b], P. Vitulo[a,b]

INFN Sezione di Perugia[a], Università di Perugia[b], Perugia, Italy
L. Alunni Solestizi[a,b], G. M. Bilei[a], D. Ciangottini[a,b], L. Fanò[a,b], P. Lariccia[a,b], R. Leonardi[a,b], G. Mantovani[a,b], M. Menichelli[a], A. Saha[a], A. Santocchia[a,b]

INFN Sezione di Pisa[a], Università di Pisa[b], Scuola Normale Superiore di Pisa[c], Pisa, Italy
K. Androsov[a,29], P. Azzurri[a,15], G. Bagliesi[a], J. Bernardini[a], T. Boccali[a], R. Castaldi[a], M. A. Ciocci[a,29], R. Dell'Orso[a], S. Donato[a,c], G. Fedi, A. Giassi[a], M. T. Grippo[a,29], F. Ligabue[a,c], T. Lomtadze[a], L. Martini[a,b], A. Messineo[a,b], F. Palla[a], A. Rizzi[a,b], A. Savoy-Navarro[a,30], P. Spagnolo[a], R. Tenchini[a], G. Tonelli[a,b], A. Venturi[a], P. G. Verdini[a]

INFN Sezione di Roma[a], Università di Roma[b], Rome, Italy
L. Barone[a,b], F. Cavallari[a], G. D'imperio[a,b,15], D. Del Re[a,b,15], M. Diemoz[a], S. Gelli[a,b], C. Jorda[a], E. Longo[a,b], F. Margaroli[a,b], P. Meridiani[a], G. Organtini[a,b], R. Paramatti[a], F. Preiato[a,b], S. Rahatlou[a,b], C. Rovelli[a], F. Santanastasio[a,b]

INFN Sezione di Torino[a], Università di Torino[b], Turin, Italy, Università del Piemonte Orientale[c], Novara, Italy
N. Amapane[a,b], R. Arcidiacono[a,c,15], S. Argiro[a,b], M. Arneodo[a,c], N. Bartosik[a], R. Bellan[a,b], C. Biino[a], N. Cartiglia[a], M. Costa[a,b], R. Covarelli[a,b], A. Degano[a,b], N. Demaria[a], L. Finco[a,b], B. Kiani[a,b], C. Mariotti[a], S. Maselli[a], E. Migliore[a,b], V. Monaco[a,b], E. Monteil[a,b], M. M. Obertino[a,b], L. Pacher[a,b], N. Pastrone[a], M. Pelliccioni[a], G. L. Pinna Angioni[a,b], F. Ravera[a,b], A. Romero[a,b], M. Ruspa[a,c], R. Sacchi[a,b], V. Sola[a], A. Solano[a,b], A. Staiano[a], P. Traczyk[a,b]

INFN Sezione di Trieste[a], Università di Trieste[b], Trieste, Italy
S. Belforte[a], V. Candelise[a,b], M. Casarsa[a], F. Cossutti[a], G. Della Ricca[a,b], C. La Licata[a,b], A. Schizzi[a,b], A. Zanetti[a]

Kangwon National University, Chunchon, Korea
S. K. Nam

Kyungpook National University, Daegu, Korea
D. H. Kim, G. N. Kim, M. S. Kim, D. J. Kong, S. Lee, S. W. Lee, Y. D. Oh, A. Sakharov, D. C. Son, Y. C. Yang

Chonbuk National University, Jeonju, Korea
J. A. Brochero Cifuentes, H. Kim, T. J. Kim[31]

Institute for Universe and Elementary Particles, Chonnam National University, Kwangju, Korea
S. Song

Korea University, Seoul, Korea
S. Cho, S. Choi, Y. Go, D. Gyun, B. Hong, Y. Jo, Y. Kim, B. Lee, K. Lee, K. S. Lee, S. Lee, J. Lim, S. K. Park, Y. Roh

Seoul National University, Seoul, Korea
H. D. Yoo

University of Seoul, Seoul, Korea
M. Choi, H. Kim, H. Kim, J. H. Kim, J. S. H. Lee, I. C. Park, G. Ryu, M. S. Ryu

Sungkyunkwan University, Suwon, Korea
Y. Choi, J. Goh, D. Kim, E. Kwon, J. Lee, I. Yu

Vilnius University, Vilnius, Lithuania
V. Dudenas, A. Juodagalvis, J. Vaitkus

National Centre for Particle Physics, Universiti Malaya, Kuala Lumpur, Malaysia
I. Ahmed, Z. A. Ibrahim, J. R. Komaragiri, M. A. B. Md Ali[32], F. Mohamad Idris[33], W. A. T. Wan Abdullah, M. N. Yusli, Z. Zolkapli

Centro de Investigacion y de Estudios Avanzados del IPN, Mexico City, Mexico
E. Casimiro Linares, H. Castilla-Valdez, E. De La Cruz-Burelo, I. Heredia-De La Cruz[34], A. Hernandez-Almada, R. Lopez-Fernandez, J. Mejia Guisao, A. Sanchez-Hernandez

Universidad Iberoamericana, Mexico City, Mexico
S. Carrillo Moreno, F. Vazquez Valencia

Benemerita Universidad Autonoma de Puebla, Puebla, Mexico
I. Pedraza, H. A. Salazar Ibarguen, C. Uribe Estrada

Universidad Autónoma de San Luis Potosí, San Luis Potosí, Mexico
A. Morelos Pineda

University of Auckland, Auckland, New Zealand
D. Krofcheck

University of Canterbury, Christchurch, New Zealand
P. H. Butler

National Centre for Physics, Quaid-I-Azam University, Islamabad, Pakistan
A. Ahmad, M. Ahmad, Q. Hassan, H. R. Hoorani, W. A. Khan, T. Khurshid, M. Shoaib, M. Waqas

National Centre for Nuclear Research, Swierk, Poland
H. Bialkowska, M. Bluj, B. Boimska, T. Frueboes, M. Górski, M. Kazana, K. Nawrocki, K. Romanowska-Rybinska, M. Szleper, P. Zalewski

Faculty of Physics, Institute of Experimental Physics, University of Warsaw, Warsaw, Poland
G. Brona, K. Bunkowski, A. Byszuk[35], K. Doroba, A. Kalinowski, M. Konecki, J. Krolikowski, M. Misiura, M. Olszewski, M. Walczak

Laboratório de Instrumentação e Física Experimental de Partículas, Lisbon, Portugal
P. Bargassa, C. Beirão Da Cruz E Silva, A. Di Francesco, P. Faccioli, P. G. Ferreira Parracho, M. Gallinaro, J. Hollar, N. Leonardo, L. Lloret Iglesias, M. V. Nemallapudi, F. Nguyen, J. Rodrigues Antunes, J. Seixas, O. Toldaiev, D. Vadruccio, J. Varela, P. Vischia

Joint Institute for Nuclear Research, Dubna, Russia
S. Afanasiev, I. Golutvin, A. Kamenev, V. Karjavin, V. Korenkov, A. Lanev, A. Malakhov, V. Matveev[36,37], V. V. Mitsyn, P. Moisenz, V. Palichik, V. Perelygin, S. Shmatov, S. Shulha, N. Skatchkov, V. Smirnov, E. Tikhonenko, N. Voytishin, A. Zarubin

Petersburg Nuclear Physics Institute, Gatchina, St. Petersburg, Russia
V. Golovtsov, Y. Ivanov, V. Kim[38], E. Kuznetsova[39], P. Levchenko, V. Murzin, V. Oreshkin, I. Smirnov, V. Sulimov, L. Uvarov, S. Vavilov, A. Vorobyev

Institute for Nuclear Research, Moscow, Russia
Yu. Andreev, A. Dermenev, S. Gninenko, N. Golubev, A. Karneyeu, M. Kirsanov, N. Krasnikov, A. Pashenkov, D. Tlisov, A. Toropin

Institute for Theoretical and Experimental Physics, Moscow, Russia
V. Epshteyn, V. Gavrilov, N. Lychkovskaya, V. Popov, I. Pozdnyakov, G. Safronov, A. Spiridonov, M. Toms, E. Vlasov, A. Zhokin

National Research Nuclear University 'Moscow Engineering Physics Institute' (MEPhI), Moscow, Russia
R. Chistov, M. Danilov, O. Markin, E. Popova, V. Rusinov

P.N. Lebedev Physical Institute, Moscow, Russia
V. Andreev, M. Azarkin[37], I. Dremin[37], M. Kirakosyan, A. Leonidov[37], G. Mesyats, S. V. Rusakov

Skobeltsyn Institute of Nuclear Physics, Lomonosov Moscow State University, Moscow, Russia
A. Baskakov, A. Belyaev, E. Boos, M. Dubinin[40], L. Dudko, A. Ershov, A. Gribushin, V. Klyukhin, O. Kodolova, I. Lokhtin, I. Miagkov, S. Obraztsov, S. Petrushanko, V. Savrin, A. Snigirev

State Research Center of Russian Federation, Institute for High Energy Physics, Protvino, Russia
I. Azhgirey, I. Bayshev, S. Bitioukov, V. Kachanov, A. Kalinin, D. Konstantinov, V. Krychkine, V. Petrov, R. Ryutin, A. Sobol, L. Tourtchanovitch, S. Troshin, N. Tyurin, A. Uzunian, A. Volkov

Faculty of Physics and Vinca Institute of Nuclear Sciences, University of Belgrade, Belgrade, Serbia
P. Adzic[41], P. Cirkovic, D. Devetak, J. Milosevic, V. Rekovic

Centro de Investigaciones Energéticas Medioambientales y Tecnológicas (CIEMAT), Madrid, Spain
J. Alcaraz Maestre, E. Calvo, M. Cerrada, M. Chamizo Llatas, N. Colino, B. De La Cruz, A. Delgado Peris, A. Escalante Del Valle, C. Fernandez Bedoya, J. P. Fernández Ramos, J. Flix, M. C. Fouz, P. Garcia-Abia, O. Gonzalez Lopez, S. Goy Lopez, J. M. Hernandez, M. I. Josa, E. Navarro De Martino, A. Pérez-Calero Yzquierdo, J. Puerta Pelayo, A. Quintario Olmeda, I. Redondo, L. Romero, M. S. Soares

Universidad Autónoma de Madrid, Madrid, Spain
J. F. de Trocóniz, M. Missiroli, D. Moran

Universidad de Oviedo, Oviedo, Spain
J. Cuevas, J. Fernandez Menendez, S. Folgueras, I. Gonzalez Caballero, E. Palencia Cortezon, J. M. Vizan Garcia

Instituto de Física de Cantabria (IFCA), CSIC-Universidad de Cantabria, Santander, Spain
I. J. Cabrillo, A. Calderon, J. R. Castiñeiras De Saa, E. Curras, M. Fernandez, J. Garcia-Ferrero, G. Gomez, A. Lopez Virto, J. Marco, R. Marco, C. Martinez Rivero, F. Matorras, J. Piedra Gomez, T. Rodrigo, A. Y. Rodríguez-Marrero, A. Ruiz-Jimeno, L. Scodellaro, N. Trevisani, I. Vila, R. Vilar Cortabitarte

CERN, European Organization for Nuclear Research, Geneva, Switzerland
D. Abbaneo, E. Auffray, G. Auzinger, M. Bachtis, P. Baillon, A. H. Ball, D. Barney, A. Benaglia, L. Benhabib, G. M. Berruti, P. Bloch, A. Bocci, A. Bonato, C. Botta, H. Breuker, T. Camporesi, R. Castello, M. Cepeda, G. Cerminara, M. D'Alfonso, D. d'Enterria, A. Dabrowski, V. Daponte, A. David, M. De Gruttola, F. De Guio, A. De Roeck, E. Di Marco[42], M. Dobson, M. Dordevic, B. Dorney, T. du Pree, D. Duggan, M. Dünser, N. Dupont, A. Elliott-Peisert, S. Fartoukh, G. Franzoni, J. Fulcher, W. Funk, D. Gigi, K. Gill, M. Girone, F. Glege, R. Guida, S. Gundacker, M. Guthoff, J. Hammer, P. Harris, J. Hegeman, V. Innocente, P. Janot, H. Kirschenmann, V. Knünz, M. J. Kortelainen, K. Kousouris, P. Lecoq, C. Lourenço, M. T. Lucchini, N. Magini, L. Malgeri, M. Mannelli, A. Martelli, L. Masetti, F. Meijers, S. Mersi, E. Meschi, F. Moortgat, S. Morovic, M. Mulders, H. Neugebauer, S. Orfanelli[43], L. Orsini, L. Pape, E. Perez, M. Peruzzi, A. Petrilli, G. Petrucciani, A. Pfeiffer, M. Pierini, D. Piparo, A. Racz, T. Reis, G. Rolandi[44], M. Rovere, M. Ruan, H. Sakulin, J. B. Sauvan, C. Schäfer, C. Schwick, M. Seidel, A. Sharma, P. Silva, M. Simon, P. Sphicas[45], J. Steggemann, M. Stoye, Y. Takahashi, D. Treille, A. Triossi, A. Tsirou, V. Veckalns[46], G. I. Veres[17], N. Wardle, H. K. Wöhri, A. Zagozdzinska[35], W. D. Zeuner

Paul Scherrer Institut, Villigen, Switzerland
W. Bertl, K. Deiters, W. Erdmann, R. Horisberger, Q. Ingram, H. C. Kaestli, D. Kotlinski, U. Langenegger, T. Rohe

Institute for Particle Physics, ETH Zurich, Zurich, Switzerland
F. Bachmair, L. Bäni, L. Bianchini, B. Casal, G. Dissertori, M. Dittmar, M. Donegà, P. Eller, C. Grab, C. Heidegger, D. Hits, J. Hoss, G. Kasieczka, P. Lecomte†, W. Lustermann, B. Mangano, M. Marionneau, P. Martinez Ruiz del Arbol, M. Masciovecchio, M. T. Meinhard, D. Meister, F. Micheli, P. Musella, F. Nessi-Tedaldi, F. Pandolfi, J. Pata, F. Pauss, G. Perrin, L. Perrozzi, M. Quittnat, M. Rossini, M. Schönenberger, A. Starodumov[47], M. Takahashi, V. R. Tavolaro, K. Theofilatos, R. Wallny

Universität Zürich, Zurich, Switzerland
T. K. Aarrestad, C. Amsler[48], L. Caminada, M. F. Canelli, V. Chiochia, A. De Cosa, C. Galloni, A. Hinzmann, T. Hreus, B. Kilminster, C. Lange, J. Ngadiuba, D. Pinna, G. Rauco, P. Robmann, D. Salerno, Y. Yang

National Central University, Chung-Li, Taiwan
K. H. Chen, T. H. Doan, Sh. Jain, R. Khurana, M. Konyushikhin, C. M. Kuo, W. Lin, Y. J. Lu, A. Pozdnyakov, S. S. Yu

National Taiwan University (NTU), Taipei, Taiwan
Arun Kumar, P. Chang, Y. H. Chang, Y. W. Chang, Y. Chao, K. F. Chen, P. H. Chen, C. Dietz, F. Fiori, W.-S. Hou, Y. Hsiung, Y. F. Liu, R.-S. Lu, M. Miñano Moya, J. F. Tsai, Y. M. Tzeng

Department of Physics, Faculty of Science, Chulalongkorn University, Bangkok, Thailand
B. Asavapibhop, K. Kovitanggoon, G. Singh, N. Sri manobhas, N. Suwonjandee

Physics Department, Science and Art Faculty, Cukurova University, Adana, Turkey
A. Adiguzel, S. Cerci[49], S. Damarseckin, Z. S. Demiroglu, C. Dozen, I. Dumanoglu, E. Eskut, S. Girgis, G. Gokbulut, Y. Guler, E. Gurpinar, I. Hos, E. E. Kangal[50], A. Kayis Topaksu, G. Onengut[51], K. Ozdemir[52], S. Ozturk[53], A. Polatoz, C. Zorbilmez

Physics Department, Middle East Technical University, Ankara, Turkey
B. Bilin, S. Bilmis, B. Isildak[54], G. Karapinar[29], M. Yalvac, M. Zeyrek

Bogazici University, Istanbul, Turkey
E. Gülmez, M. Kaya[56], O. Kaya[57], E. A. Yetkin[58], T. Yetkin[59]

Istanbul Technical University, Istanbul, Turkey
A. Cakir, K. Cankocak, S. Sen[60]

Institute for Scintillation Materials, National Academy of Science of Ukraine, Kharkov, Ukraine
B. Grynyov

National Scientific Center, Kharkov Institute of Physics and Technology, Kharkov, Ukraine
L. Levchuk, P. Sorokin

University of Bristol, Bristol, UK
R. Aggleton, F. Ball, L. Beck, J. J. Brooke, D. Burns, E. Clement, D. Cussans, H. Flacher, J. Goldstein, M. Grimes, G. P. Heath, H. F. Heath, J. Jacob, L. Kreczko, C. Lucas, Z. Meng, D. M. Newbold[61], S. Paramesvaran, A. Poll, T. Sakuma, S. Seif El Nasr-storey, S. Senkin, D. Smith, V. J. Smith

Rutherford Appleton Laboratory, Didcot, UK
K. W. Bell, A. Belyaev[62], C. Brew, R. M. Brown, L. Calligaris, D. Cieri, D. J. A. Cockerill, J. A. Coughlan, K. Harder, S. Harper, E. Olaiya, D. Petyt, C. H. Shepherd-Themistocleous, A. Thea, I. R. Tomalin, T. Williams, S. D. Worm

Imperial College, London, UK
M. Baber, R. Bainbridge, O. Buchmuller, A. Bundock, D. Burton, S. Casasso, M. Citron, D. Colling, L. Corpe, P. Dauncey, G. Davies, A. De Wit, M. Della Negra, P. Dunne, A. Elwood, D. Futyan, Y. Haddad, G. Hall, G. Iles, R. Lane, R. Lucas[61], L. Lyons, A.-M. Magnan, S. Malik, L. Mastrolorenzo, J. Nash, A. Nikitenko[47], J. Pela, B. Penning, M. Pesaresi, D. M. Raymond, A. Richards, A. Rose, C. Seez, A. Tapper, K. Uchida, M. Vazquez Acosta[63], T. Virdee[15], S. C. Zenz

Brunel University, Uxbridge, UK
J. E. Cole, P. R. Hobson, A. Khan, P. Kyberd, D. Leslie, I. D. Reid, P. Symonds, L. Teodorescu, M. Turner

Baylor University, Waco, USA
A. Borzou, K. Call, J. Dittmann, K. Hatakeyama, H. Liu, N. Pastika

The University of Alabama, Tuscaloosa, USA
O. Charaf, S. I. Cooper, C. Henderson, P. Rumerio

Boston University, Boston, USA
D. Arcaro, A. Avetisyan, T. Bose, D. Gastler, D. Rankin, C. Richardson, J. Rohlf, L. Sulak, D. Zou

Brown University, Providence, USA
J. Alimena, G. Benelli, E. Berry, D. Cutts, A. Ferapontov, A. Garabedian, J. Hakala, U. Heintz, O. Jesus, E. Laird, G. Landsberg, Z. Mao, M. Narain, S. Piperov, S. Sagir, R. Syarif

University of California, Davis, Davis, USA
R. Breedon, G. Breto, M. Calderon De La Barca Sanchez, S. Chauhan, M. Chertok, J. Conway, R. Conway, P. T. Cox, R. Erbacher, C. Flores, G. Funk, M. Gardner, W. Ko, R. Lander, C. Mclean, M. Mulhearn, D. Pellett, J. Pilot, F. Ricci-Tam, S. Shalhout, J. Smith, M. Squires, D. Stolp, M. Tripathi, S. Wilbur, R. Yohay

University of California, Los Angeles, USA
R. Cousins, P. Everaerts, A. Florent, J. Hauser, M. Ignatenko, D. Saltzberg, E. Takasugi, V. Valuev, M. Weber

University of California, Riverside, Riverside, USA
K. Burt, R. Clare, J. Ellison, J. W. Gary, G. Hanson, J. Heilman, P. Jandir, E. Kennedy, F. Lacroix, O. R. Long, M. Malberti, M. Olmedo Negrete, M. I. Paneva, A. Shrinivas, H. Wei, S. Wimpenny, B. R. Yates

University of California, San Diego, La Jolla, USA
J. G. Branson, G. B. Cerati, S. Cittolin, R. T. D'Agnolo, M. Derdzinski, R. Gerosa, A. Holzner, R. Kelley, D. Klein, J. Letts, I. Macneill, D. Olivito, S. Padhi, M. Pieri, M. Sani, V. Sharma, S. Simon, M. Tadel, A. Vartak, S. Wasserbaech[64], C. Welke, J. Wood, F. Würthwein, A. Yagil, G. Zevi Della Porta

Department of Physics, University of California, Santa Barbara, Santa Barbara, USA
J. Bradmiller-Feld, C. Campagnari, A. Dishaw, V. Dutta, K. Flowers, M. Franco Sevilla, P. Geffert, C. George, F. Golf, L. Gouskos, J. Gran, J. Incandela, N. Mccoll, S. D. Mullin, J. Richman, D. Stuart, I. Suarez, C. West, J. Yoo

California Institute of Technology, Pasadena, USA
D. Anderson, A. Apresyan, J. Bendavid, A. Bornheim, J. Bunn, Y. Chen, J. Duarte, A. Mott, H. B. Newman, C. Pena, M. Spiropulu, J. R. Vlimant, S. Xie, R. Y. Zhu

Carnegie Mellon University, Pittsburgh, USA
M. B. Andrews, V. Azzolini, A. Calamba, B. Carlson, T. Ferguson, M. Paulini, J. Russ, M. Sun, H. Vogel, I. Vorobiev

University of Colorado Boulder, Boulder, USA
J. P. Cumalat, W. T. Ford, F. Jensen, A. Johnson, M. Krohn, T. Mulholland, K. Stenson, S. R. Wagner

Cornell University, Ithaca, USA
J. Alexander, A. Chatterjee, J. Chaves, J. Chu, S. Dittmer, N. Eggert, N. Mirman, G. Nicolas Kaufman, J. R. Patterson, A. Rinkevicius, A. Ryd, L. Skinnari, L. Soffi, W. Sun, S. M. Tan, W. D. Teo, J. Thom, J. Thompson, J. Tucker, Y. Weng, P. Wittich

Fermi National Accelerator Laboratory, Batavia, USA
S. Abdullin, M. Albrow, G. Apollinari, S. Banerjee, L. A. T. Bauerdick, A. Beretvas, J. Berryhill, P. C. Bhat, G. Bolla, K. Burkett, J. N. Butler, H. W. K. Cheung, F. Chlebana, S. Cihangir, M. Cremonesi, V. D. Elvira, I. Fisk, J. Freeman, E. Gottschalk, L. Gray, D. Green, S. Grünendahl, O. Gutsche, D. Hare, R. M. Harris, S. Hasegawa, J. Hirschauer, Z. Hu, B. Jayatilaka, S. Jindariani, M. Johnson, U. Joshi, B. Klima, B. Kreis, S. Lammel, J. Lewis, J. Linacre, D. Lincoln, R. Lipton, T. Liu, R. Lopes De Sá, J. Lykken, K. Maeshima, J. M. Marraffino, S. Maruyama, D. Mason, P. McBride, P. Merkel, S. Mrenna, S. Nahn, C. Newman-Holmes†, V. O'Dell, K. Pedro, O. Prokofyev, G. Rakness, E. Sexton-Kennedy, A. Soha, W. J. Spalding, L. Spiegel, S. Stoynev, N. Strobbe, L. Taylor, S. Tkaczyk, N. V. Tran, L. Uplegger, E. W. Vaandering, C. Vernieri, M. Verzocchi, R. Vidal, M. Wang, H. A. Weber, A. Whitbeck

University of Florida, Gainesville, USA
D. Acosta, P. Avery, P. Bortignon, D. Bourilkov, A. Brinkerhoff, A. Carnes, M. Carver, D. Curry, S. Das, R. D. Field, I. K. Furic, J. Konigsberg, A. Korytov, K. Kotov, P. Ma, K. Matchev, H. Mei, P. Milenovic[65], G. Mitselmakher, D. Rank, R. Rossin, L. Shchutska, D. Sperka, N. Terentyev, L. Thomas, J. Wang, S. Wang, J. Yelton

Florida International University, Miami, USA
S. Linn, P. Markowitz, G. Martinez, J. L. Rodriguez

Florida State University, Tallahassee, USA
A. Ackert, J. R. Adams, T. Adams, A. Askew, S. Bein, J. Bochenek, B. Diamond, J. Haas, S. Hagopian, V. Hagopian, K. F. Johnson, A. Khatiwada, H. Prosper, A. Santra, M. Weinberg

Florida Institute of Technology, Melbourne, USA
M. M. Baarmand, V. Bhopatkar, S. Colafranceschi[66], M. Hohlmann, H. Kalakhety, D. Noonan, T. Roy, F. Yumiceva

University of Illinois at Chicago (UIC), Chicago, USA
M. R. Adams, L. Apanasevich, D. Berry, R. R. Betts, I. Bucinskaite, R. Cavanaugh, O. Evdokimov, L. Gauthier, C. E. Gerber, D. J. Hofman, P. Kurt, C. O'Brien, I. D. Sandoval Gonzalez, P. Turner, N. Varelas, Z. Wu, M. Zakaria, J. Zhang

The University of Iowa, Iowa City, USA
B. Bilki[67], W. Clarida, K. Dilsiz, S. Durgut, R. P. Gandrajula, M. Haytmyradov, V. Khristenko, J.-P. Merlo, H. Mermerkaya[68], A. Mestvirishvili, A. Moeller, J. Nachtman, H. Ogul, Y. Onel, F. Ozok[69], A. Penzo, C. Snyder, E. Tiras, J. Wetzel, K. Yi

Johns Hopkins University, Baltimore, USA
I. Anderson, B. Blumenfeld, A. Cocoros, N. Eminizer, D. Fehling, L. Feng, A. V. Gritsan, P. Maksimovic, M. Osherson, J. Roskes, U. Sarica, M. Swartz, M. Xiao, Y. Xin, C. You

The University of Kansas, Lawrence, USA
P. Baringer, A. Bean, C. Bruner, J. Castle, R. P. Kenny III, A. Kropivnitskaya, D. Majumder, M. Malek, W. Mcbrayer, M. Murray, S. Sanders, R. Stringer, Q. Wang

Kansas State University, Manhattan, USA
A. Ivanov, K. Kaadze, S. Khalil, M. Makouski, Y. Maravin, A. Mohammadi, L. K. Saini, N. Skhirtladze, S. Toda

Lawrence Livermore National Laboratory, Livermore, USA
D. Lange, F. Rebassoo, D. Wright

University of Maryland, College Park, USA
C. Anelli, A. Baden, O. Baron, A. Belloni, B. Calvert, S. C. Eno, C. Ferraioli, J. A. Gomez, N. J. Hadley, S. Jabeen, R. G. Kellogg, T. Kolberg, J. Kunkle, Y. Lu, A. C. Mignerey, Y. H. Shin, A. Skuja, M. B. Tonjes, S. C. Tonwar

Massachusetts Institute of Technology, Cambridge, USA
A. Apyan, R. Barbieri, A. Baty, R. Bi, K. Bierwagen, S. Brandt, W. Busza, I. A. Cali, Z. Demiragli, L. Di Matteo, G. Gomez Ceballos, M. Goncharov, D. Gulhan, D. Hsu, Y. Iiyama, G. M. Innocenti, M. Klute, D. Kovalskyi, K. Krajczar, Y. S. Lai, Y.-J. Lee, A. Levin, P. D. Luckey, A. C. Marini, C. Mcginn, C. Mironov, S. Narayanan, X. Niu, C. Paus, C. Roland, G. Roland, J. Salfeld-Nebgen, G. S. F. Stephans, K. Sumorok, K. Tatar, M. Varma, D. Velicanu, J. Veverka, J. Wang, T. W. Wang, B. Wyslouch, M. Yang, V. Zhukova

University of Minnesota, Minneapolis, USA
A. C. Benvenuti, B. Dahmes, A. Evans, A. Finkel, A. Gude, P. Hansen, S. Kalafut, S. C. Kao, K. Klapoetke, Y. Kubota, Z. Lesko, J. Mans, S. Nourbakhsh, N. Ruckstuhl, R. Rusack, N. Tambe, J. Turkewitz

University of Mississippi, Oxford, USA
J. G. Acosta, S. Oliveros

University of Nebraska-Lincoln, Lincoln, USA
E. Avdeeva, R. Bartek, K. Bloom, S. Bose, D. R. Claes, A. Dominguez, C. Fangmeier, R. Gonzalez Suarez, R. Kamalieddin, D. Knowlton, I. Kravchenko, F. Meier, J. Monroy, F. Ratnikov, J. E. Siado, G. R. Snow, B. Stieger

State University of New York at Buffalo, Buffalo, USA
M. Alyari, J. Dolen, J. George, A. Godshalk, C. Harrington, I. Iashvili, J. Kaisen, A. Kharchilava, A. Kumar, A. Parker, S. Rappoccio, B. Roozbahani

Northeastern University, Boston, USA
G. Alverson, E. Barberis, D. Baumgartel, M. Chasco, A. Hortiangtham, A. Massironi, D. M. Morse, D. Nash, T. Orimoto, R. Teixeira De Lima, D. Trocino, R.-J. Wang, D. Wood, J. Zhang

Northwestern University, Evanston, USA
S. Bhattacharya, K. A. Hahn, A. Kubik, J. F. Low, N. Mucia, N. Odell, B. Pollack, M. H. Schmitt, K. Sung, M. Trovato, M. Velasco

University of Notre Dame, Notre Dame, USA
N. Dev, M. Hildreth, C. Jessop, D. J. Karmgard, N. Kellams, K. Lannon, N. Marinelli, F. Meng, C. Mueller, Y. Musienko[36], M. Planer, A. Reinsvold, R. Ruchti, N. Rupprecht, G. Smith, S. Taroni, N. Valls, M. Wayne, M. Wolf, A. Woodard

The Ohio State University, Columbus, USA
L. Antonelli, J. Brinson, B. Bylsma, L. S. Durkin, S. Flowers, A. Hart, C. Hill, R. Hughes, W. Ji, B. Liu, W. Luo, D. Puigh, M. Rodenburg, B. L. Winer, H. W. Wulsin

Princeton University, Princeton, USA
O. Driga, P. Elmer, J. Hardenbrook, P. Hebda, S. A. Koay, P. Lujan, D. Marlow, T. Medvedeva, M. Mooney, J. Olsen, C. Palmer, P. Piroué, D. Stickland, C. Tully, A. Zuranski

University of Puerto Rico, Mayaguez, USA
S. Malik

Purdue University, West Lafayette, USA
A. Barker, V. E. Barnes, D. Benedetti, L. Gutay, M. K. Jha, M. Jones, A. W. Jung, K. Jung, D. H. Miller, N. Neumeister, B. C. Radburn-Smith, X. Shi, J. Sun, A. Svyatkovskiy, F. Wang, W. Xie, L. Xu

Purdue University Calumet, Hammond, USA
N. Parashar, J. Stupak

Rice University, Houston, USA
A. Adair, B. Akgun, Z. Chen, K. M. Ecklund, F. J. M. Geurts, M. Guilbaud, W. Li, B. Michlin, M. Northup, B. P. Padley, R. Redjimi, J. Roberts, J. Rorie, Z. Tu, J. Zabel

University of Rochester, Rochester, USA
B. Betchart, A. Bodek, P. de Barbaro, R. Demina, Y. t. Duh, Y. Eshaq, T. Ferbel, M. Galanti, A. Garcia-Bellido, J. Han, O. Hindrichs, A. Khukhunaishvili, K. H. Lo, P. Tan, M. Verzetti

Rutgers, The State University of New Jersey, Piscataway, USA
J. P. Chou, E. Contreras-Campana, Y. Gershtein, T. A. Gómez Espinosa, E. Halkiadakis, M. Heindl, D. Hidas, E. Hughes, S. Kaplan, R. Kunnawalkam Elayavalli, S. Kyriacou, A. Lath, K. Nash, H. Saka, S. Salur, S. Schnetzer, D. Sheffield, S. Somalwar, R. Stone, S. Thomas, P. Thomassen, M. Walker

University of Tennessee, Knoxville, USA
M. Foerster, J. Heideman, G. Riley, K. Rose, S. Spanier, K. Thapa

Texas A&M University, College Station, USA
O. Bouhali[70], A. Castaneda Hernandez[70], A. Celik, M. Dalchenko, M. De Mattia, A. Delgado, S. Dildick, R. Eusebi, J. Gilmore, T. Huang, T. Kamon[71], V. Krutelyov, R. Mueller, I. Osipenkov, Y. Pakhotin, R. Patel, A. Perloff, L. Perniè, D. Rathjens, A. Rose, A. Safonov, A. Tatarinov, K. A. Ulmer

Texas Tech University, Lubbock, USA
N. Akchurin, C. Cowden, J. Damgov, C. Dragoiu, P. R. Dudero, J. Faulkner, S. Kunori, K. Lamichhane, S. W. Lee, T. Libeiro, S. Undleeb, I. Volobouev, Z. Wang

Vanderbilt University, Nashville, USA
E. Appelt, A. G. Delannoy, S. Greene, A. Gurrola, R. Janjam, W. Johns, C. Maguire, Y. Mao, A. Melo, H. Ni, P. Sheldon, S. Tuo, J. Velkovska, Q. Xu

University of Virginia, Charlottesville, USA
M. W. Arenton, P. Barria, B. Cox, B. Francis, J. Goodell, R. Hirosky, A. Ledovskoy, H. Li, C. Neu, T. Sinthuprasith, X. Sun, Y. Wang, E. Wolfe, F. Xia

Wayne State University, Detroit, USA
C. Clarke, R. Harr, P. E. Karchin, C. Kottachchi Kankanamge Don, P. Lamichhane, J. Sturdy

University of Wisconsin-Madison, Madison, WI, USA
D. A. Belknap, D. Carlsmith, S. Dasu, L. Dodd, S. Duric, B. Gomber, M. Grothe, M. Herndon, A. Hervé, P. Klabbers, A. Lanaro, A. Levine, K. Long, R. Loveless, A. Mohapatra, I. Ojalvo, T. Perry, G. A. Pierro, G. Polese, T. Ruggles, T. Sarangi, A. Savin, A. Sharma, N. Smith, W. H. Smith, D. Taylor, P. Verwilligen, N. Woods

Tata Institute of Fundamental Research, Mumbai, India
T. Aziz, S. Banerjee, S. Bhowmik[72], R. M. Chatterjee, R. K. Dewanjee, S. Dugad, S. Ganguly, S. Ghosh, M. Guchait, A. Gurtu[73], Sa. Jain, G. Kole, S. Kumar, B. Mahakud, M. Maity[72], G. Majumder, K. Mazumdar, S. Mitra, G. B. Mohanty, B. Parida, T. Sarkar[72], N. Sur, B. Sutar, N. Wickramage[74]

† **Deceased**

1: Also at Vienna University of Technology, Vienna, Austria
2: Also at State Key Laboratory of Nuclear Physics and Technology, Peking University, Beijing, China
3: Also at Institut Pluridisciplinaire Hubert Curien, Université de Strasbourg, Université de Haute Alsace Mulhouse, CNRS/IN2P3, Strasbourg, France
4: Also at Universidade Estadual de Campinas, Campinas, Brazil
5: Also at Centre National de la Recherche Scientifique (CNRS)-IN2P3, Paris, France
6: Also at Université Libre de Bruxelles, Brussels, Belgium
7: Also at Laboratoire Leprince-Ringuet, Ecole Polytechnique, IN2P3-CNRS, Palaiseau, France

8: Also at Joint Institute for Nuclear Research, Dubna, Russia
9: Also at Helwan University, Cairo, Egypt
10: Now at Zewail City of Science and Technology, Zewail, Egypt
11: Now at Ain Shams University, Cairo, Egypt
12: Also at Fayoum University, El-Fayoum, Egypt
13: Now at British University in Egypt, Cairo, Egypt
14: Also at Université de Haute Alsace, Mulhouse, France
15: Also at CERN, European Organization for Nuclear Research, Geneva, Switzerland
16: Also at Skobeltsyn Institute of Nuclear Physics, Lomonosov Moscow State University, Moscow, Russia
17: Also at Tbilisi State University, Tbilisi, Georgia
18: Also at Ilia State University, Tbilisi, Georgia
19: Also at RWTH Aachen University, III. Physikalisches Institut A, Aachen, Germany
20: Also at University of Hamburg, Hamburg, Germany
21: Also at Brandenburg University of Technology, Cottbus, Germany
22: Also at Institute of Nuclear Research ATOMKI, Debrecen, Hungary
23: Also at MTA-ELTE Lendület CMS Particle and Nuclear Physics Group, Eötvös Loránd University, Budapest, Hungary
24: Also at Institute of Physics, University of Debrecen, Debrecen, Hungary
25: Also at Indian Institute of Science Education and Research, Bhopal, India
26: Also at Isfahan University of Technology, Isfahan, Iran
27: Also at University of Tehran, Department of Engineering Science, Tehran, Iran
28: Also at Plasma Physics Research Center, Science and Research Branch, Islamic Azad University, Tehran, Iran
29: Also at Università degli Studi di Siena, Siena, Italy
30: Also at Purdue University, West Lafayette, USA
31: Now at Hanyang University, Seoul, Korea
32: Also at International Islamic University of Malaysia, Kuala Lumpur, Malaysia
33: Also at Malaysian Nuclear Agency, MOSTI, Kajang, Malaysia
34: Also at Consejo Nacional de Ciencia y Tecnología, Mexico City, Mexico
35: Also at Warsaw University of Technology, Institute of Electronic Systems, Warsaw, Poland
36: Also at Institute for Nuclear Research, Moscow, Russia
37: Now at National Research Nuclear University 'Moscow Engineering Physics Institute' (MEPhI), Moscow, Russia
38: Also at St. Petersburg State Polytechnical University, St. Petersburg, Russia
39: Also at University of Florida, Gainesville, USA
40: Also at California Institute of Technology, Pasadena, USA
41: Also at Faculty of Physics, University of Belgrade, Belgrade, Serbia
42: Also at INFN Sezione di Roma, Università di Roma, Rome, Italy
43: Also at National Technical University of Athens, Athens, Greece
44: Also at Scuola Normale e Sezione dell'INFN, Pisa, Italy
45: Also at National and Kapodistrian University of Athens, Athens, Greece
46: Also at Riga Technical University, Riga, Latvia
47: Also at Institute for Theoretical and Experimental Physics, Moscow, Russia
48: Also at Albert Einstein Center for Fundamental Physics, Bern, Switzerland
49: Also at Adiyaman University, Adiyaman, Turkey
50: Also at Mersin University, Mersin, Turkey
51: Also at Cag University, Mersin, Turkey
52: Also at Piri Reis University, Istanbul, Turkey
53: Also at Gaziosmanpasa University, Tokat, Turkey
54: Also at Ozyegin University, Istanbul, Turkey
55: Also at Izmir Institute of Technology, Izmir, Turkey
56: Also at Marmara University, Istanbul, Turkey
57: Also at Kafkas University, Kars, Turkey
58: Also at Istanbul Bilgi University, Istanbul, Turkey
59: Also at Yildiz Technical University, Istanbul, Turkey
60: Also at Hacettepe University, Ankara, Turkey

61: Also at Rutherford Appleton Laboratory, Didcot, UK
62: Also at School of Physics and Astronomy, University of Southampton, Southampton, UK
63: Also at Instituto de Astrofísica de Canarias, La Laguna, Spain
64: Also at Utah Valley University, Orem, USA
65: Also at University of Belgrade, Faculty of Physics and Vinca Institute of Nuclear Sciences, Belgrade, Serbia
66: Also at Facoltà Ingegneria, Università di Roma, Rome, Italy
67: Also at Argonne National Laboratory, Argonne, USA
68: Also at Erzincan University, Erzincan, Turkey
69: Also at Mimar Sinan University, Istanbul, Istanbul, Turkey
70: Also at Texas A&M University at Qatar, Doha, Qatar
71: Also at Kyungpook National University, Daegu, Korea
72: Also at University of Visva-Bharati, Santiniketan, India
73: Now at King Abdulaziz University, Jeddah, Saudi Arabia
74: Also at University of Ruhuna, Matara, Sri Lanka